Androgen Receptor Regulation of Germ Cell Migration across Sertoli Cell Tight Junctions

Benjamin E. Smith

A dissertation

submitted in partial fulfillment of the

requirements for the degree of

Doctor of Philosophy

University of Washington

2012

Reading Committee:

Robert E. Braun, Chair

Leo Pallanck

Richard D. Palmiter

Program Authorized to Offer Degree:

Genome Sciences

Abstract

Androgen Receptor Regulation of Germ Cell Migration across Sertoli Cell Tight Junctions

Benjamin E. Smith

Chair of the Supervisory Committee:
Professor Robert E. Braun
Genome Sciences

The blood-testis barrier includes a tight junction barrier between Sertoli cells that restricts solutes of varying size and charge from crossing the paracellular space thus enabling the formation of unique microenvironments within seminiferous tubules and providing immune privilege to meiotic and postmeiotic cells. Remarkably, large syncytial chains of germ cells are able to transit the Sertoli cell tight junctions (SCTJs) without compromising their integrity. We studied how germ cell cysts migrate across the SCTJs using confocal microscopy to visualize the interplay of SCTJ components during the transit event. Consequently, we were able to determine that the germ cells accomplish this remarkable feat by becoming briefly enclosed within a network of transient compartments fully-bounded by old tight junctions on the adluminal side and new tight junctions on the basal side. We also found that claudin-3 (CLDN3), a tight junction protein, is transiently incorporated into new tight junctions and that formation of new tight junctions is disrupted in mice lacking androgen signaling in somatic Sertoli cells. We followed up on these initial discoveries by generating mice that had floxed *Cldn3* locus. To our surprise, we found that *Cldn3* knockout mice were fertile and had an intact SCTJ barrier. We then further investigated the expression of tight junction components in mice lacking androgen signaling in somatic Sertoli cells, and found that several tight junction components we down-regulated in these mice in addition to *Cldn3,* including *Cldn13, Cldn20, Tjp1* and *Tjp2* isoform C.

TABLE OF CONTENTS

LIST OF FIGURES

CHAPTER I: GERM CELL MIGRATION ACROSS SERTOLI CELL TIGHT JUNCTIONS

CHAPTER II: ANDROGEN RECEPTOR REGULATION OF SERTOLI CELL TIGHT JUNCTION REMODELING IS INDEPENDENT OF CLAUDIN-3

LIST OF TABLES

CHAPTER II: ANDROGEN RECEPTOR REGULATION OF SERTOLI CELL TIGHT JUNCTION REMODELING IS INDEPENDENT OF CLAUDIN-3

GLOSSARY

Blood-testis barrier – A series of tight junction barriers between the circulatory system and the adluminal compartment of the seminiferous tubules. The blood-testis barrier includes tight junctions between the endothelial cell of the blood vessels, incomplete tight junctions between the peritubular myoid cells, and tight junctions between the Sertoli cells.

Peritubular myoid cells – Smooth muscle-like cells that surround the seminiferous tubules and form the basement memebrane of the seminiferous tubules.

Seminiferous tubules – Long tubules that form the bulk of the testis, where spermatogonia divide and differentiate to form spermatids.

Sertoli cells – The primary somatic cell within the seminiferous tubules that feeds and supports the developing germ cells.

Spermatid – A haploid male germ cell that will mature within the epididymus to form mature spermatozoa.

Spermatocyte – A diploid meiotic male germ cell derived from spermatogonia, which undergoes meiosis to form spermatids.

Spermatogenic wave – A repeating series of coordinated germ cell differentiation steps that form down the length of the seminiferous tubule, ensuring continuous sperm production.

Spermatogonium – A diploid stem cell precursor of spermatozoa that reside on the basement membrane of seminiferous tubules.

Stages of spermatogenesis – Sequential divisions of the spermatogenic wave that are identified by a unique and reproducible combination of subtypes of spermatogonia, spermatocytes, and spermatids. There are twelve such stages that make up the mouse spermatogenic wave.

Tight junctions – A protein based cell-cell adhesion structure that occludes the intercellular space.

ACKNOWLEDGEMENTS

The author would like to express his gratitude both to his thesis committee and the faculty and staff at the Jackson Laboratory, especially Mary-Ann Handel, for helping to interpret data and to formulate ideas. This thesis was also dependent upon the training and time offered by James Denegre and Mark Lessard on the techniques of high-resolution confocal imaging and using image rendering software. The author would also like to thank his wife and family for their support and encouragement.

DEDICATION

In memory of Jezz

INTRODUCTION

The existence of a blood-testis barrier was first postulated by Hugo Ribbert (Ribbert, 1904), when after injecting rabbits with carmine, he noted that the brain, oocytes, and seminiferous tubules were not labeled by carmine, unlike all other tissues in the body. In conjunction with recent discovery that the brain was not labeled by dyes injected into the circulatory system or subcutaneously due to a physical barrier between the blood and the brain (Lewandowsky, 1900), Dr. Ribbert's discovery was the first to suggest that there was a comparable barrier within the seminiferous tubules.

The exact nature and location of the blood-testis barrier was characterized in much finer detail in a pair of studies by Dr. Martin Dym (Dym and Cavicchia, 1977; Dym and Fawcett, 1970). In the first study (Dym and Fawcett, 1970), an electron dense lanthanum colloid was perfused throughout rats, and then the testes were examined via transmission electron microscopy. Tight junction structures were found within the blood vessels in the testis, as well as between most of the peritubular myoid cells (the cells that make up the basement membrane of the seminiferous tubules), and between all Sertoli cells. The lanthanum colloid was able to readily pass through the endothelial tight junctions, but was blocked by both the peritubular myoid cell tight junctions and the Sertoli cells tight junctions. In a similar follow-up study in macaques, it was found that as germ cells migrated across the Sertoli cell tight junctions (SCTJs) towards the adluminal compartment, a new tight junction formed on the basal side of the migrating cell. This new tight junction

was also found to be sufficient to prevent the SCTJ barrier from breaking during the migration, thus the SCTJ barrier remained intact at all times.

The most recent breakthrough in tight junction biology came from a pair of studies in 1998 that found that tight junctions were formed by the claudin family of proteins (Furuse et al., 1998a; Furuse et al., 1998b). This opened up the field of tight junction biology, and just a year later it was discovered that claudin-11 (CLDN11) was a critical component of the SCTJs (Gow et al., 1999; Morita et al., 1999b).

Another claudin, claudin-3 (CLDN3), was also found to be transiently associated with the SCTJs (Meng et al., 2005). When studying testis transcripts that were differentially regulated in mice that were deficient in androgen receptor (*Ar)* expression (Holdcraft and Braun, 2004a), *Cldn3* was found to be down-regulated in mice that lacked AR expression in the testis. Follow-up analysis demonstrated that not only was CLDN3 localized to the SCTJs, but that it was also under the direct regulation of AR. As a result, CLDN3 was transiently associated with the SCTJs, coinciding with peak AR expression in Sertoli cells. Functional studies of the SCTJ barrier demonstrated that even though CLDN11 was still present in the SCTJs, the SCTJ barrier was compromised in mice that lacked AR expression in Sertoli cells (Meng et al., 2005; Willems et al., 2010). These mice were also found to have autoimmune orchitis, further suggesting the SCTJ barrier is compromised (Meng et al., 2011).

CHAPTER I: GERM CELL MIGRATION ACROSS SERTOLI CELL TIGHT JUNCTIONS

Abstract:

The blood-testis barrier includes a tight junction barrier between Sertoli cells that restricts solutes of varying size and charge from crossing the paracellular space thus enabling the formation of unique microenvironments within seminiferous tubules and providing immune priviledge to meiotic and postmeiotic cells. Remarkably, large clonal syncytial chains of germ cells are able to transit the Sertoli cell tight junctions (SCTJs) without compromising their integrity. We studied how germ cell cysts migrate across the SCTJ using confocal microscopy to visualize the interplay of SCTJ components during the transit event. Consequently, we were able to determine that the germ cells accomplish this remarkable feat via the equivalent of an air-lock mechanism by becoming briefly enclosed within a network of transient compartments fully-bounded by old tight junctions on the adluminal side and new tight junctions on the basal side. We also found that claudin-3, a tight junction protein, is transiently incorporated into new tight junctions and that formation of new tight junctions is disrupted in mice lacking androgen signaling in somatic Sertoli cells.

Introduction:

Tight junctions are specialized anchoring junctions, composed of several integral and peripheral membrane proteins (Schneeberger and Lynch, 2004; Tsukita et al., 2001). The elaborate fibrils formed by the tight junction components play a critical role in multi-cellular organisms by sealing off the space between neighboring epithelial cells thereby partitioning compartments within an organism (Tsukita et al., 2008). They also help create and maintain apical to basal polarity within epithelial cells and regulate the diffusion of solutes of varying charge and size across epithelia. Claudins, four-pass integral membrane proteins, are the main tight junction components and the only proteins known that can form tight junctions *de novo* in cell culture (Furuse et al., 1998b).Twenty-four different claudins have been described since the initial discovery of *Cldn1* and *Cldn2* in the late nineties (Furuse et al., 1998a). The claudin-based tight junction fibrils are fortified and anchored to the cytoskeleton by the zona occludens, which link the C-terminal tails of claudins with filamentous-actin, resulting in characteristic F-actin bundles that shadow the tight junction fibrils (Furuse, 2010).

Tight junctions are dynamic structures, whose composition can be altered in response to external factors, resulting in changes in their barrier properties. One such external factor is when other cells either extend pseudopodia through tight junctions, or transmigrate completely across the tight junctions. Two mechanisms of single cell transmigration across tight junctions are known. When individual basal cells extend pseudopodia across epididymal and tracheal tight junctions, they form their own tight junctions with the neighboring epithelial cells, therefore

preserving the integrity of the tight junction barrier (Shum et al., 2008). During inflammatory responses in the brain, the tight junction protein claudin-3 (CLDN3), is selectively down-regulated, allowing leukocytes to cross the blood-brain barrier (Wolburg et al., 2003).

Spermatogenesis is a lengthy and highly ordered process of cellular differentiation that takes place within seminiferous tubules of the testis. Extensive tight junctions between somatic Sertoli cells create two compartments within the tubular epithelium; a basal compartment demarcated by the basal lamina at the tubule circumference, and an adluminal compartment that extends to the lumen of the tubule (Figure 1a). The basal compartment segregates the diploid spermatogonia from the more differentiated meiotic and postmeiotic germ cells. All spermatogonia occupy the basal compartment, lie along the basal lamina of the epithelium and are in direct contact with somatic Sertoli cells. As these cells proliferate and differentiate they do not complete cytokinesis, instead forming long syncitial chains of cells that detach from the basement membrane and translocate to the lumen of the tubule, where haploid spermatids are released (Huckins, 1978). The basal and adluminal compartments created by the Sertoli cell tight junctions help establish and maintain unique microenviroments for germ cells at varying stages of differentiation (Griswold, 1998).

Sertoli cell tight junctions are unusual in several ways. Unlike other polarized epithelia, where the tight junctions are apical, the seminiferous epithelium is reversed; the tight junctions are on the basal side of the epithelium. In addition, the seminiferous epithelium is the only known epithelium that is regularly traversed by

another cell type – chains of long preleptotene spermatocytes. This reversed epithelium and the periodic translocation by preleptotene spermatocytes provide unique challenges in protein trafficking and tight junction remodeling.

Sertoli cell tight junctions (SCTJs) are comprised of Claudin-11 (CLDN11), zonula occludins-1 (ZO-1), occludin (Morita et al., 1999b) and several other accessory proteins. Targeted deletion of *Cldn11* causes a complete loss of the SCTJs and infertility (Gow et al., 1999). A second member of the claudin family, *Cldn3,* is transiently associated with the SCTJ during tight junction remodeling and preleptotene spermatocyte transit (Meng et al., 2005). Tight junction remodeling is regulated by androgens via expression of the androgen receptor in Sertoli cells (Meng et al., 2005) and Sertoli cell-specific ablation of the androgen receptor results in loss of immune-privilege and increased permeability to solutes (Meng et al., 2011; Meng et al., 2005; Willems et al., 2010).

Classical transmission electron microscopy (TEM) and lanthanum tracer studies demonstrated that the SCTJ barrier remains functionally intact during germ cell translocation from the basal to the adluminal compartment (Dym and Cavicchia, 1977). Direct observation of the SCTJs revealed that as the preleptotene spermatocytes begin their transmigration, new SCTJs form on the basal side of the migrating cells, suggesting the formation of an intermediate compartment (Russell, 1977). Despite these early elegant studies, the mechanism by which large synctial chains of preleptotene spermatocytes move from the basal to the adluminal compartment without disrupting the functional integrity of the SCTJs has remained a mystery for more than four decades.

In this study, we used confocal microscopy on intact seminiferous tubules to visualize the 3-dimensional (3-D) organization of the SCTJs. We imaged the SCTJs prior to and during translocation of the preleptotene spermatocytes from the basal to the adluminal compartment. We also determined the subcellular localization of CLDN3, which is transiently associated with SCTJs during spermatocyte translocation, and characterized the SCTJ defects present in mice lacking androgen receptor signaling in Sertoli cells. Our data suggests that syncitial chains of preleptotene spermatocytes are enclosed within the SCTJs via an interconnected transient network of smaller compartments.

Results:

Preleptotene spermatocytes are enclosed within a transient intermediate compartment bounded by tight junctions

To visualize the 3D organization of the SCTJs, we stained seminiferous tubules of 10-week old B6129PF1/J mice for claudin-11 (CLDN11) and F-actin, both of which are known constituents of the SCTJs (Morita et al., 1999b; Russell et al., 1989). The tubules were then imaged by confocal microscopy from the basal surface to approximately 15μm into the tubule in 150 to 200 optical sections (Figure 1a).

First, we imaged regions of the seminiferous tubules where no germ cells were migrating across the SCTJs. Filamentous-actin, labeled with phalloidin, and CLDN11 both marked the SCTJs, while the phalloidin also labeled other F-actin rich structures, including peritubular myoid cells and elongated spermatids (Figure 1b). Individual Sertoli cells were bounded on their entire circumference by CLDN11 fibrils and were usually in contact with five to seven other Sertoli cells. In these regions, CLDN11 circumscribed each Sertoli cell near the basement membrane (Figure 1c), and delineated the basal and adluminal compartments by passing between the spermatogonia and pachytene spermatocytes (Figure 1d). Gaps in CLDN11 staining were never detected confirming the functional integrity of the SCTJs throughout the epithelium.

We then imaged regions of the seminiferous tubules where preleptotene spermatocytes were migrating across the SCTJs, using spermiation (release of

spermatids into the lumen) as a marker for this transit (Oakberg, 1956). During preleptotene spermatocyte translocation across the SCTJs, CLDN11 tight junctions were observed on both the basal and adluminal sides of the migrating spermatocytes (Figure 2a). This double-layered tight junction was observed only enclosing preleptotene spermatocytes, and these tight junctions merged to form a single SCTJ where there were no migrating spermatocytes. Additionally, we observed vertical cross-linked connections between the basal and adluminal tight junction strands, enclosing the spermatocytes in a network of subcompartments. These vertical tight junctions were found only at the tricellular junctions of three Sertoli cells (Figure 2a arrowhead), possibly suggesting a role of the specialized tight junction structures in the formation of these compartments (Masuda et al., 2011). Therefore, as previously suggested (Russell, 1977), preleptotene spermatocytes are temporarily enclosed in an intermediate compartment bounded by CLDN11 on all sides (Figure 2b).

Because preleptotene spermatocytes are syncytial, forming long cysts of cells joined by cytoplasmic bridges (Weber and Russell, 1987), and the compartments we observed generally contained only two preleptotene spermatocytes, we hypothesized that the cytoplasmic bridges must pass between the enclosed compartments at the regions of the tricellular junctions. To image cysts of preleptotene spermatocytes in the context of the SCTJ compartments, seminiferous tubules were stained with both CLDN11 and testis-expressed gene 14 (TEX14), which localizes to a portion of each cytoplasmic bridge (Greenbaum et al., 2006). As expected, TEX14 was observed between cells within individual compartments, and

as hypothesized, we observed intercellular bridges, marked by TEX14, proximal to the tricellular junctions (Figure 2a arrowhead). These data suggest that large chains of syncytial germ cells span several smaller compartments (Figure 2c). The intercellular bridges connecting germ cells within a cyst pass through the smaller compartments that are linked to ultimately comprise a single large compartment of one intact cyst.

New Sertoli-Sertoli cell contact allows for the remodeling of the SCTJs

The SCTJs form only at Sertoli-Sertoli cell contacts (Dym and Fawcett, 1970). Therefore, our observation that migrating preleptotene spermatocytes are bounded both apically and basally by SCTJs, suggests that the basal surface of the Sertoli cells form new Sertoli-Sertoli cell contacts to accommodate the formation of the new tight junctions. To visualize the 3D structure of the Sertoli cells, we generated mice that express EGFP only within the cytoplasm of Sertoli cells by crossing Tg(ACTB-Bgeo/GFP)21Lbe/J (Z/EG) mice with 129S.FVB-Tg(Amh-cre)8815Reb/J (Amh-Cre) mice. The seminiferous tubules from the resulting Z/EG; Amh-Cre F1 male progeny were then stained for EGFP to visualize the Sertoli cell body, and CLDN11 and F-actin, to visualize the SCTJs.

Sertoli cell contacts with the basement membrane and with each other change during the course of the spermatogenic cycle. Prior to preleptotene migration across the SCTJs, we observed the basal surfaces of Sertoli cells adhered to the basement membrane, except where spermatogonia were present (Figure 3a). To accommodate spermatogonia that were also bound to the basement membrane,

the basal surfaces of neighboring Sertoli cells were displaced away from the basement membrane, cradling the spermatogonia in trough-like structures (Figure 3a). The SCTJs were present at the Sertoli-Sertoli cell contacts just below the spermatogonia (not shown). As spermatogonia continue to proliferate and differentiate, the chains of cells expand between the Sertoli cells, such that by stage VII of spermatogenesis, the basal surfaces of the Sertoli cells no longer contact one another (Figure 3b). As the preleptotene cells lose contact with the basement membrane, the basal surface of the Sertoli cells intercalate between the preleptotene spermatocytes (now leptoneme spermatocytes) and the basement membrane (Figure 3c), enclosing the migrating spermatocytes in a tunnel-like structure (Figure 3d). This change in Sertoli cell shape also allows for the formation of new Sertoli-Sertoli cell contacts and new tight junctions on the basal side of the leptotene spermatocytes.

CLDN3 localizes to the newly forming SCTJ

A remarkable feature of the remodeling of the SCTJs is that the Sertoli cells are able to form a new tight junction at the correct place, on the basal side of migrating preleptotene spermatocytes, and at the correct time, immediately after the formation of a new Sertoli-Sertoli contact. We have previously shown that CLDN3 is transiently expressed at the time of SCTJ remodeling and translocation of preleptotene spermatocytes from the basal to the adluminal compartment (Meng et al., 2005).

To determine where CLDN3 localizes in the SCTJs, we stained adult seminiferous tubules for CLDN3 and with F-actin as a marker for the SCTJs. The earliest stage of spermatogenesis in which we observed CLDN3 staining was Stage VII, which is just prior to the preleptonema migration and agrees with previous studies (Meng et al., 2005). Interestingly, rather than localizing to the SCTJs as expected, CLDN3 was distributed across the basal surface of the Sertoli cells (Figure 4a), consistent with the observation that there are no Sertoli-Sertoli cell contacts on the basal surface of Sertoli cells at this stage to allow for tight junction formation.

At stage VIII-IX of spermatogenesis, when the preleptotene spermatocytes are crossing the SCTJs, CLDN3 was no longer distributed on the basal surface and was observed to be integrated into SCTJs (Figure 4b). Specifically, CLDN3 was localized to the newly forming tight junction at the new Sertoli-Sertoli cell contacts near the basement membrane, bridging gaps in the SCTJs where migrating preleptotene spermatocytes were being enclosed in the SCTJs. By stage XI, when the leptotene spermatocytes emerge into the adluminal compartment, CLDN3 was absent from the seminiferous tubule, leaving behind a new SCTJ, with the leptotene spermatocytes having now emerged into the adluminal compartment (Figure 4c).

Sertoli cell tight junction remodeling is compromised in an androgen receptor mouse model

We have previously shown that in mice lacking the androgen receptor in Sertoli cells, $Ar^{invflox(ex1\text{-}neo)}$; Amh-Cre, , the permeability of the SCTJs is increased (Meng et al., 2005) and the testis is immune compromised (Meng et al., 2011).

Previous characterization of these mice had determined that they had reduced CLDN3 expression in Sertoli cells but CLDN11 expression was mainly unaffected (Meng et al., 2005). Despite the presence of CLDN11 in all the seminiferous tubules, the SCTJ barrier was compromised in adult males (Meng et al., 2005).

Initial investigation of the structure of the SCTJs revealed a barrier with no gross breaks or disorganization (Figure 5a). However, during spermatocyte migration, CLDN11 staining no longer circumscribed each Sertoli cell, and instead was seen as a disorganized mass of protein, poorly resembling a SCTJ network (Figure 5b). After spermatocyte migration, CLDN11 expression gradually transitioned from its disorganized pattern, seeming to reassemble the damaged tight junctions. This apparent "destruction" of the SCTJs was observed only when preleptotene spermatocytes were crossing the SCTJ barrier, suggesting that the previously observed permeability of the SCTJ barrier may be in part explained by a failure to properly remodel the SCTJs during the transmigration, instead resulting in a complete disruption of the barrier.

Discussion

We have shown that syncytial chains of preleptotene spermatocytes become transiently enclosed within the SCTJs via a network of transient subcompartments, sealed by vertical tight junction strands that form at tricellular junctions. By visualizing a portion of the cytoplasmic bridges using TEX14, we were able to conclude that the intercellular bridges that connect germ cells within a syncytium span neighboring compartments by crossing the tricellular junctions, thereby allowing a complete syncytium to remain intact while also being enclosed within the SCTJs.

Classical early electron micrographic studies had suggested the existence of an intermediate tight junction compartment for migrating preleptotene spermatocytes (Chihara et al., 2010; Dym and Cavicchia, 1977; Dym and Fawcett, 1970; Russell, 1977). However, the inability to follow cells within a germ cell cyst in micrographs prohibited these early investigators from addressing the critical issue of movement of entire chains of preleptotene spermatocytes across the SCTJs. In addition, others have failed to find more than one occluding zonule per Sertoli cell (Cavicchia and Sacerdote, 1988; Pelletier and Friend, 1983), an expectation if an intermediate compartment exists. More recently, additional models have been suggested for the passage of germ cells across SCTJs (Mruk and Cheng, 2004). By compiling hundreds of optical confocal sections taken from whole mount seminiferous tubules immunostained for CLDN11, our data conclusively demonstrate the existence of an intermediate compartment. Moreover, our studies

resolve the issue of movement of an entire syncytium and provide insight into the molecular and cellular mechanism of new tight junction formation.

In previous studies we showed that CLDN3 was transiently expressed and associated with SCTJs during their remodeling in stages VIII – IX of the spermatogenic cycle (Meng et al., 2005). We asked here whether CLDN3 is localized to the new tight junctions on the basal side of the leptotene spermatocytes, in which case it would most likely function in the initiation of new tight junction formation, or whether it is present on the apical side of the leptotene spermatocytes, in which case it might function in the dissolution of the old tight junctions. Contrary to previous studies on histological sections (Chihara et al., 2010), we observed CLDN3 localization on the basal surface of Sertoli cells and exclusively localized to the newly forming SCTJs just prior to germ cell migration. By also determining how the basal surfaces of the Sertoli cells are remodeled during the migration, we conclude that new tight junction formation is dependent on new Sertoli cell contacts during the critical stages. Based on these findings we propose an "air-lock" model for spermatocyte translocation across the SCTJs (Figure 4d). As the preleptotene spermatocytes lose contact with the basement membrane, the basal membrane of the Sertoli cells is loaded with CLDN3 (Stage VII). The Sertoli cells then intercalate between the basement membrane and the preleptotene spermatocytes, and new CLDN3 tight junctions form at regions of Sertoli-Sertoli cell contact (Stage VIII). CLDN11 tight junctions then replace CLDN3, enclosing the chains of preleptotene spermatocytes within the SCTJs (Stage IX-X). Once the chain is fully enclosed within

the SCTJ, the ”old” tight junctions are removed, releasing the leptotene spermatocytes into the adluminal compartment (Stage XI-XII).

New tight junction formation requires asymmetric localization of CLDN3 to the basal surface, detachment of preleptotene spermatocytes from the basement membrane and extension of Sertoli cells between the basement membrane and preleptotene spermatocytes. An interesting question remains of how CLDN3 is selectively trafficked to the basal surface of Sertoli cells just prior to the migration. Note, however, that because the basal surface of the Sertoli cells are “preloaded” with CLDN3, new tight junctions are formed wherever new Sertoli-Sertoli cell contacts form in the basal compartment. Because these new contacts form only behind migrating spermatocytes, CLDN3 tight junctions form behind the migrating spermatocytes, thus forming new tight junction fibrils only where needed.

Regions of new tight junction formation contain both CLDN3 and CLDN11. Our data do not allow us to definitively conclude whether formation of CLDN3 TJs precede CLDN11 TJs, or whether the proteins form new tight junctions simultaneously. In cultured fibroblasts, CLDN3 is capable of forming both homotypic and heterotypic tight junctions (Furuse et al., 1999). It has also been shown that claudins are also capable of forming both homomeric and heteromeric complexes within cells (Daugherty et al., 2007). Our immunofluorescence data suggest that CLDN3 and CLDN11 form independent homotypic interactions between Sertoli cells. We also failed to observe overlap in immunostaining between CLDN3 and CLDN11 within cells, suggesting that in Sertoli cells these proteins exist as homomeric complexes.

Germ cell translocation from the basal to the adluminal compartment requires coordination of several events. Prior to germ cell migration, preleptotene spermatocytes are in direct contact with the extracellular matrix. Translocation to the adluminal compartment requires detachment from the ECM and movement toward the adluminal compartment. What regulates detachment and migration of the germ cells is unknown. Germ cells may have an intrinsic program that couples meiotic events with changes in adhesion to the ECM and migration across the SCTJs. Alternatively, Sertoli cells may regulate detachment of germ cells from the ECM and actively move germ cells between compartments. Androgens are not likely to be involved in either detachment or translocation as spermatocytes are found in the adluminal compartment in SCARKO mice (Chang et al., 2004; De Gendt et al., 2004; Holdcraft and Braun, 2004a).

We discovered that intact syncytial clones of germ cells cross the SCTJs by integrating themselves within multiple intermediate sub-compartments of CLDN11-demarcated tight junctions. Syncytial chains of cells remain intact by passage of cytoplasmic bridges between intermediate compartments at tricellular junctions. Gven the fidelity of the SCTJs in preventing movement of solutes between the basal and adluminal compartments, the protrusion of a germ cell intercellular bridge through the tricellular junction must not disrupt its functionality. Unlike the extension of pseudopodia across epididymal and tracheal tight junctions, where the basal cells themselves form tight junctions with their neighboring epithelial cells, we found no evidence of germ cells forming tight junctions with Sertoli cells. It has recently been suggested that during spermatogonial stem cell (SSCs) homing to the

niche following germ cell transplantation, where SSCs move from the adluminal to the basal compartment, that CLDN3 expression in germ cells is important for passage across or through the Sertoli cell tight junctions (Takashima et al., 2011). Contrary to these findings, we failed to detect expression of CLDN3 or CLDN11 in germ cells. Nonetheless, it remains a possibility that there may be other claudins or junctional proteins expressed in germ cells that create impermeable germ-Sertoli cell barriers at tricellular junctions.

Genetic ablation of androgen signaling in Sertoli cells leads to down regulation of CLDN3 in Sertoli cells, an increase in the permeability of the SCTJs (Meng et al., 2005) and loss of immune tolerance provided to postmeiotic germ cells (Meng et al., 2011). Recently, others have confirmed that CLDN3 levels are reduced in SCARKO mice and that restriction of solutes across the SCTJs is compromised (Willems et al., 2010). Our data here confirm the loss of CLDN3 expression in SCARKO mice and provide new insights into SCTJ remodeling in the absence of AR signaling. Upon initial investigation, we were surprised to find the SCTJs in the SCARKO mice, as assessed by CLDN11 staining, appeared structurally normal with no obvious breaks. However, when we imaged regions of seminiferous tubules where germ cells were transiting the SCTJs, we found that the CLDN11 tight junction fibrils were severely disrupted. After the initial transmigration, we observed the SCTJs progressively reassemble back to a normal organization on the basal side of the migrating germ cells. These results further confirm that androgens regulate SCTJ remodeling during germ cell migration during stages VIII-IX. The action of androgens on Sertoli cell function is therefore directly correlated with the stage-

specific expression of androgen receptor (Bremner et al., 1994). However, our studies also demonstrate that over the course of the 8.6-day seminiferous cycle that Sertoli cells are able to at least partially recover from lack of androgen signaling and correct the defect in the CLDN11 tight junction fibrils. It is tempting to speculate that CLDN3 is directly responsible for the tight junction defects in SCARKO mice. However, AR is a known regulator of many events that occur at the same time as the germ cell transmigrations, including maturation of pachytene spermatocytes, spermatid differentiation and spermiation (Holdcraft and Braun, 2004b). Androgen signaling in Sertoli cells has also been shown to regulate other junctional and cytoskeletal components in Sertoli cells (Eacker et al., 2007; Willems et al., 2010). Therefore, the extent to which CLDN3 contributes to the SCTJ phenotype awaits the conditional ablation of *Cldn3* in Sertoli cells.

Methods:

Preparing seminiferous tubule whole mounts

Protocols for the use of mice in these experiments were approved by the Jackson Laboratory Animal Care and Use Committee and in accord with National Institutes of Health standards established by the Guidelines for the Care and Use of Experimental Animals (reference). Adult (2-3 months) male 129/SvJaeSor and C57BL/6J mice were euthanized with CO_2 and the testes were immediately transferred to chilled PBS. The tunica albuginea was then removed and the seminiferous tubules were teased apart. The interstitial cells were removed by incubating the tubules in 0.5 mg/mL collagenase (Sigma) at room temperature (RT) for 5 minutes while continuing to tease the tubules apart. The tubules were then rinsed three times with PBS, and fixed in 2% paraformaldehyde (Electron Microscopy Sciences) for 6 hours at 4°C.

To observe the three-dimensional structure of Sertoli cells, a 129.B6(N1)Tg(ACTB-Bgeo/GFP)21Lbe (Z/EG) male was crossed to two 129S.FVB-Tg(Amh-cre)8815Reb/J (Amh-Cre) females. The F1 adult males that were Z/EG/+; Amh-Cre/+ were used in the study.

To observe SCTJ structure in mice deficient in AR, we crossed $Ar^{invflox(ex1)}/X$ females with Amh-Cre/Amh-Cre males. The F1 adult males that were $Ar^{invflox(ex1)}/Y$; Amh-Cre/+ were used in the study.

Immunohistochemistry on whole mounts

Paraformaldehyde-fixed tubules were rinsed three times with PBS, and permeabilized with 0.25% NP-40 (US Biologicals; city, state) in PBS-T (PBS + 0.05% Tween (Fisher Bioreagents; city, state)) for 25 minutes at RT. The tubules were rinsed three times with PBS-T, 5 minutes each, and blocked using 5% normal donkey serum (Jackson Immuno Research; city, state) in PBS-T either 2 hours at RT or over-night at 4°C. The tubules were labeled with one of the following primary antibodies diluted 1:200 in PBS-T + 5% normal donkey serum over-night at 4°C: rabbit α Cldn11 H-107 (Santa Cruz Biotechnology; city, state), rabbit α Cldn3 (Zymed; city, state), and rabbit α GFP Alexa Fluor® 488 (Molecular Probes; city, state), and rinsed three times with PBS-T, 5 minutes each. The tubules were then stained with a combination of the following secondary antibodies for 1 hour at RT: Alexa Fluor® 594 donkey α goat (Molecular Probes), Alexa Fluor® 488 donkey α rabbit (Molecular Probes), Cy3® donkey α goat (Abcam; city,state), and Alexa Fluor® 633 phalloidin (Molecular Probes), and rinsed three times with PBS-T, 5 minutes each with DAPI added to the first rinse. The tubules were spread in a drop of VectaShield® with DAPI (Vector Laboratories; city, state), covered with a coverslip, and sealed with nail polish.

Confocal microscopy of seminiferous tubules

The seminiferous tubules were imaged on a Leica® TCS SP2 laser scanning confocal microscope. The images were acquired using serial sections starting from the basement membrane and ending on the apical side of the SCTJs with an average voxel size of 150 nm x 150 nm x 150 nm. The stage of the seminiferous epithelial

cycle at which the series were taken was confirmed using both DIC and DAPI optical cross sections. The image series were rendered using the Amira® 4.1.2 software package (Visage Imaging; city, state). Heat-map colorimetrics were used, where blue light intensity, such as DAPI fluorescence, is represented on a blue to white heat map and red fluorescence, such as CLDN11, is represented on a red to bright yellow heat map. Isosurfaces were rendered using a fixed color.

Acknowledgments:

We thank Mark Lessard for assistance with confocal imaging and Jesse Hammer for artistic rendering of the images. This research was supported by a grant to REB from NICHD/NIH (HD12629) as part of the Specialized Cooperative Centers Program in Reproduction Research.

FIGURE 1.

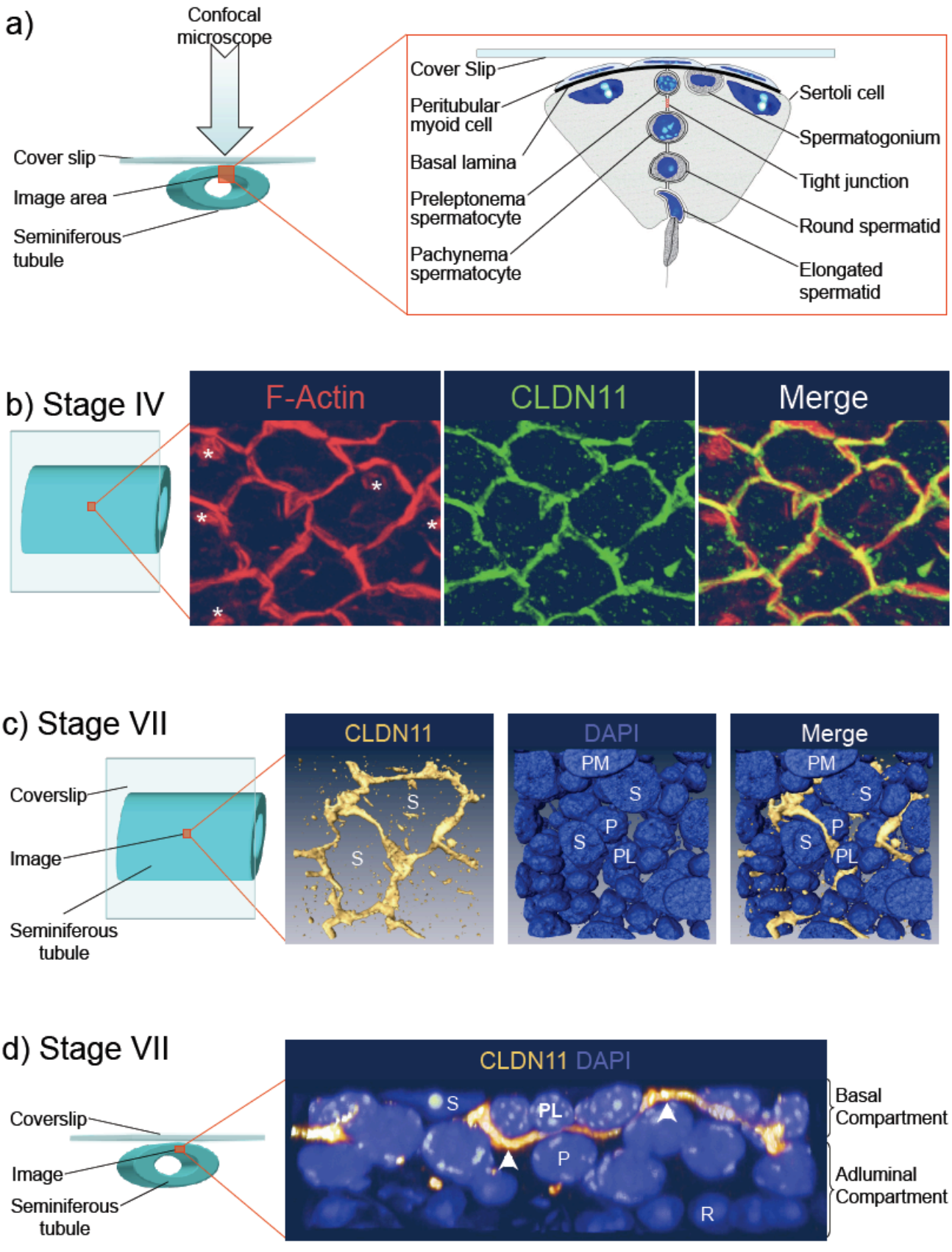
a)
Confocal microscope
Cover slip
Image area
Seminiferous tubule
Cover Slip
Peritubular myoid cell
Basal lamina
Preleptonema spermatocyte
Pachynema spermatocyte
Sertoli cell
Spermatogonium
Tight junction
Round spermatid
Elongated spermatid
b) Stage IV
F-Actin
CLDN11
Merge
c) Stage VII
Coverslip
Image
Seminiferous tubule
CLDN11
DAPI
Merge
PM
S
P
PL
d) Stage VII
Coverslip
Image
Seminiferous tubule
CLDN11 DAPI
S
PL
P
R
Basal Compartment
Adluminal Compartment

FIGURE 1. **3D organization of Sertoli cell tight junctions.** a) Whole mount seminiferous tubules were fixed, tight junction components detected by immunofluorescence and imaged with confocal microscopy. The boxed image on the right shows the organization of a seminiferous tubule in relation to the SCTJs, with the nuclei (blue) showing the DAPI staining characteristic of each cell type. b) The SCTJs were visualized using two different markers, f-actin and CLDN11. F-actin strongly labeled the SCTJs and more weakly labeled peritubular myoid cells (not shown) and near the heads of elongating spermatids (*). CLDN11 labeled just the SCTJs. The merge shows that both markers label the SCTJs. c) A 3-D isosurface reconstruction of a region of a whole seminiferous tubule stained with CLDN11 (tight junction) and DAPI (DNA). The image is viewed from the basal surface looking into the seminiferous tubule. The CLDN11 staining shows the SCTJs circumscribing each Sertoli cell (S). Preleptotene spermatocytes (PL) and peritubular myoid (PM) cells are on the basal side of the SCTJs, while pachytene spermatocytes (P) and round spermatids (not shown) are on the adluminal side of the SCTJs. d) A Z-projection of image (c) showing a cross-sectional view of the SCTJs (arrowheads) in relation to Sertoli cells (S), preleptotene (PL) and pachytene (P) spermatocytes and round spermatids (R). This figure shows that the CLDN11 staining delineates the basal and adluminal compartments of the seminiferous tubule.

FIGURE 2.

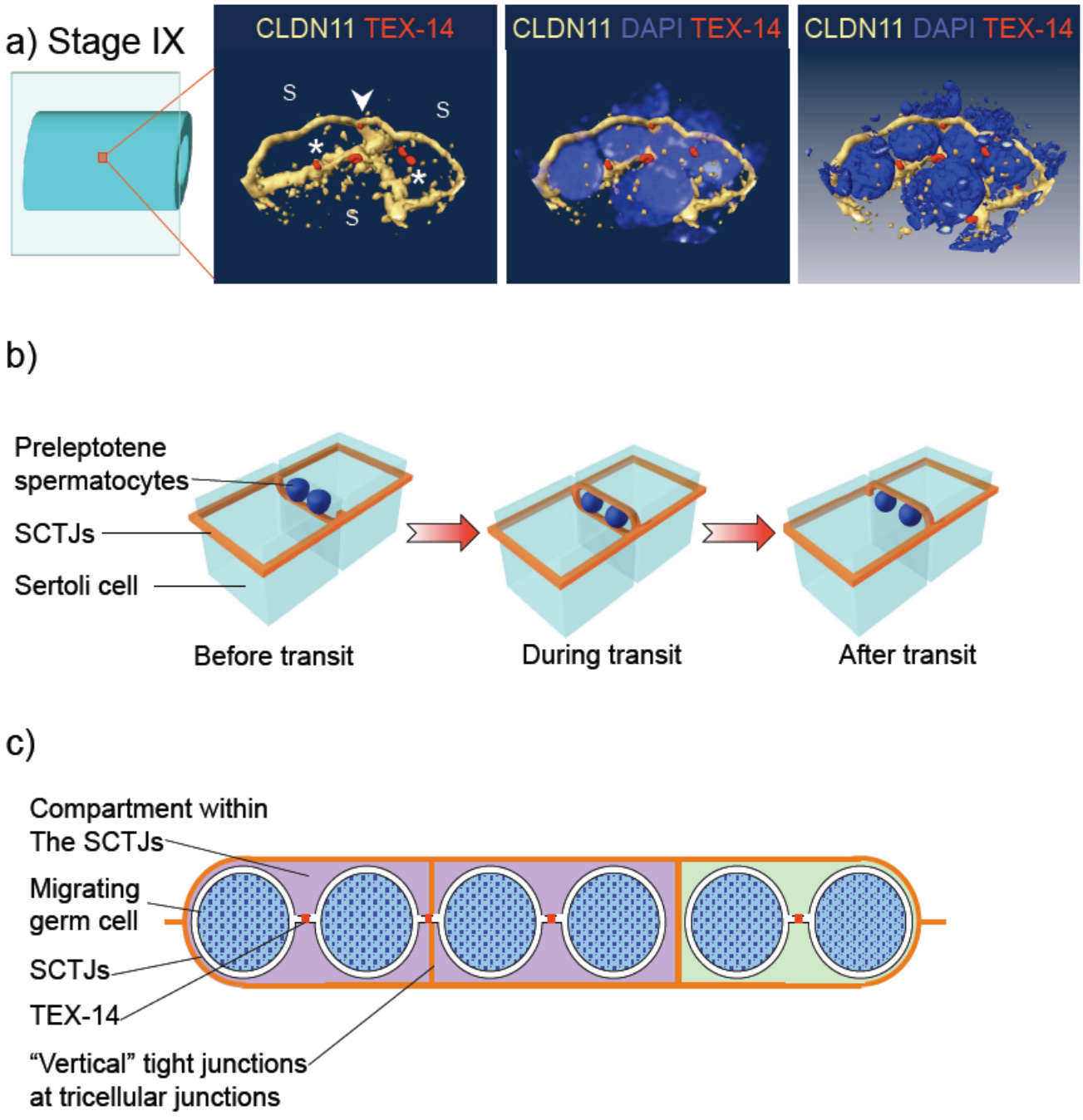
a) Stage IX
CLDN11 TEX-14
CLDN11 DAPI TEX-14
CLDN11 DAPI TEX-14
S
S
S
b)
Preleptotene spermatocytes
SCTJs
Sertoli cell
Before transit
During transit
After transit
c)
Compartment within The SCTJs
Migrating germ cell
SCTJs
TEX-14
"Vertical" tight junctions at tricellular junctions

FIGURE 2. **Migrating preleptotene spermatocytes are enclosed within the SCTJs.** a) During the migration of preleptotene spermatocytes across the SCTJs, stage XI of the seminiferous epithelium cycle, the preleptotene spermatocytes are enclosed within compartments in the SCTJs (*). The compartments are formed by a double-layer tight junction that sandwiches the preleptotene spermatocytes. The arrowhead shows connections between tight junction layers formed at tricellular meeting points of three Sertoli cells (S). TEX-14 (red) marks the cytoplasmic bridges between the preleptotene spermatocytes. TEX-14 localization to the tricellular junctions (arrowhead) reveals that the cytoplasmic bridges between spermatocytes can cross the tricellular junctions. b) A schematic of germ-cell migration across the SCTJs, showing the preleptotene spermatocytes transiently enclosed within the SCTJs before emerging into the adluminal compartment. c) A schematic of cytoplasmic bridges passing though the tricellular junctions, connecting neighboring compartments. In this schematic there are two chains of preleptotene spermatocytes, a chain of two and a chain of four (the chains are much shorter than in real-life for the sake of simplicity). The chain of two spermatocytes does not span past the SCTJs and therefore is completely enclosed within a compartment (green). The chain of four has a cytoplasmic bridge that breaches a "vertical" tight junction, however the entire chain still remains enclosed within a compartment within the SCTJs (magenta), with the described cytoplasmic bridge joining the two neighboring compartments into one large, and intact, compartment. This concept can be expanded to large clonal chains joining many compartments together and yet, still being enclosed within the SCTJs.

FIGURE 3.

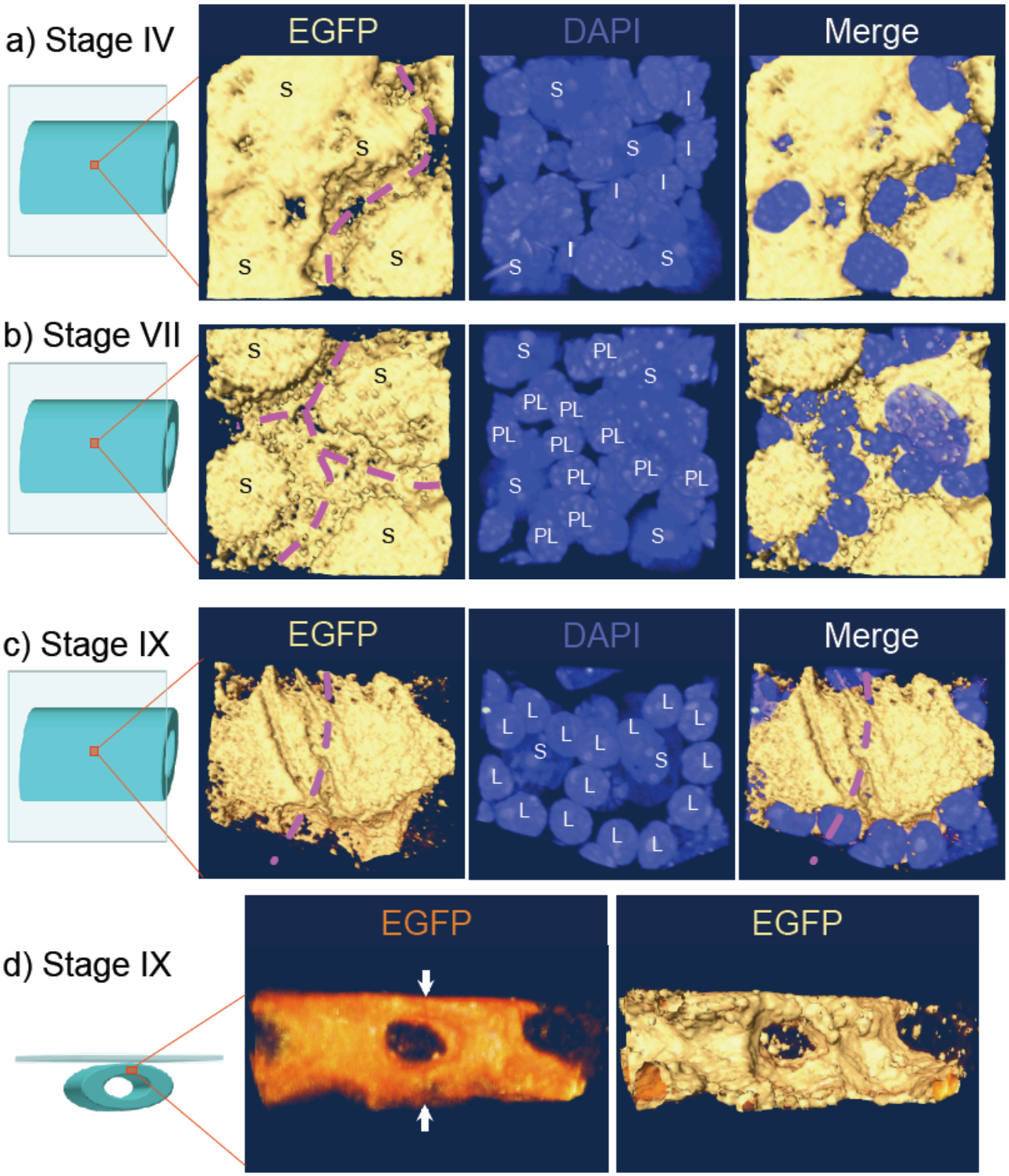
a) Stage IV
EGFP
DAPI
Merge
b) Stage VII
c) Stage IX
EGFP
DAPI
Merge
d) Stage IX
EGFP
EGFP

FIGURE 3. **Sertoli cells intercalate between migrating preleptotene spermatocytes and the basement membrane forming new Sertoli-Sertoli cell contacts.** The 3D shape of the basal surface of Sertoli cells was visualized via cytoplasmic EGFP expression (beige). a) During stage IV of the seminiferous epithelium cycle, the basal surfaces of the Sertoli cells (S) are mostly adhered to the basement membrane. Clonal chains of intermediate spermatogonia (I) reside in a trough-like structure (pink dashed line) between adjacent Sertoli cells. b) During stage VII of the seminiferous epithelium cycle, a portion of the basal surface of Sertoli cells (S) remains attached to the basement membrane. Preleptotene spermatocytes (PL), displace the basal surface of Sertoli cells such that there are no Sertoli-Sertoli cell contacts on the basal surface. c) As the leptotene spermatocytes (L) migrate away from the basement membrane and through the SCTJs, during stage IX of the seminiferous epithelium cycle, the basal surface of the Sertoli cells intercalates between the spermatocytes and the basement membrane, forming new Sertoli-Sertoli cell contacts. d) A Z-projection views of the resulting tunnel-like structures that enclose the preleptonema spermatocytes. The point of contact between the two adjacent Sertoli cells is visible (arrows).

FIGURE 4.

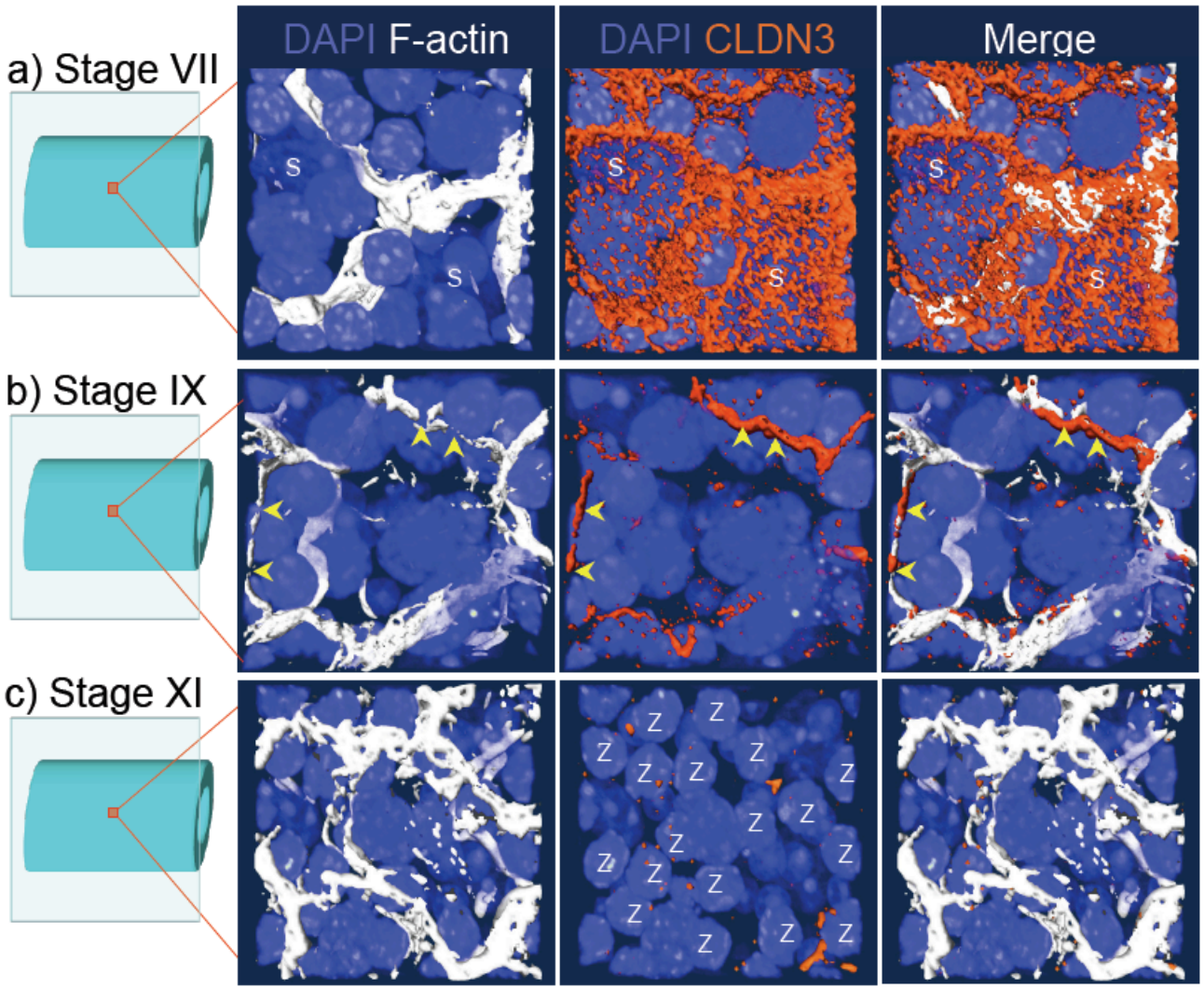
a) Stage VII
b) Stage IX
c) Stage XI
DAPI F-actin
DAPI CLDN3
Merge
S
Z

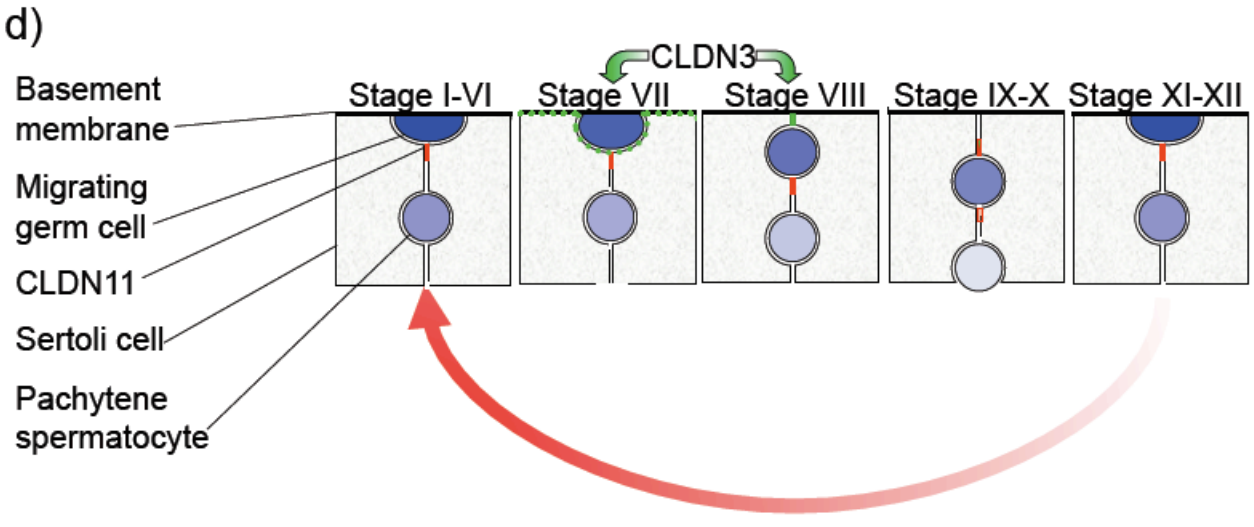
d)
Basement membrane
Migrating germ cell
CLDN11
Sertoli cell
Pachytene spermatocyte
CLDN3
Stage I-VI
Stage VII
Stage VIII
Stage IX-X
Stage XI-XII

FIGURE 4. **CLDN3 localizes to the newly forming SCTJs.** a) Just prior to the migration of preleptotene spermatocytes across the SCTJs, in stage VII of the seminiferous epithelium cycle, CLDN3 (orange) is initially localized to the basal surface of the Sertoli cells (S) rather than the SCTJs (white). b) As the preleptotene spermatocytes migrate across the SCTJs, in stage IX of the seminiferous epithelium cycle, the spermatocytes are enclosed within the SCTJs (white). However, the basal side of these compartments is incomplete as visualized as breaks in the tight junctions (yellow arrowheads). CLDN3 (orange) localizes to these breaks in the incomplete TJ structure. c) After the zygotene spermatocytes (Z) have emerged into the adluminal compartment, stage XI of the seminiferous epithelium cycle, CLDN3 (orange) has been almost completely removed from the SCTJs (white).
d) An airlock-like model for spermatocyte migration across the SCTJs. Before germ cell migration across the SCTJs, stage I-VI, the differentiating spermatogonia are in the basal compartment, adhered to the basement membrane. The tight junctions are a single layered structure (red) that delineates the basal and adluminal compartments. Just before the preleptotene spermatocytes migrate off of the basement membrane, stage VII, CLDN3 (green) is localized to the basal surface of the Sertoli cells. As there are no Sertoli-Sertoli cell contacts on the basal surface of Sertoli cells, CLDN3 cannot form a tight junction and instead remains dispersed on the basal surface. Once the preleptotene spermatocyte leaves the basement membrane, stage VIII, the basal surface of the Sertoli cells intercalates between the basement membrane and the preleptotene spermatocyte, forming a new Sertoli-Sertoli cell contact. CLDN3 (green) then localizes to this new contact and forms a

new tight junction that encloses the preleptotene spermatocytes. At stage IX, CLDN3 is gradually replaced with CLDN11 forming a new SCTJ barrier. Towards the end of stage X, the old SCTJs begin to be removed. At stage XI-XII, the zygotene spermatocytes emerge into the adluminal compartment, and a new SCTJ barrier is completely formed, allowing the cycle to repeat.

FIGURE 5.

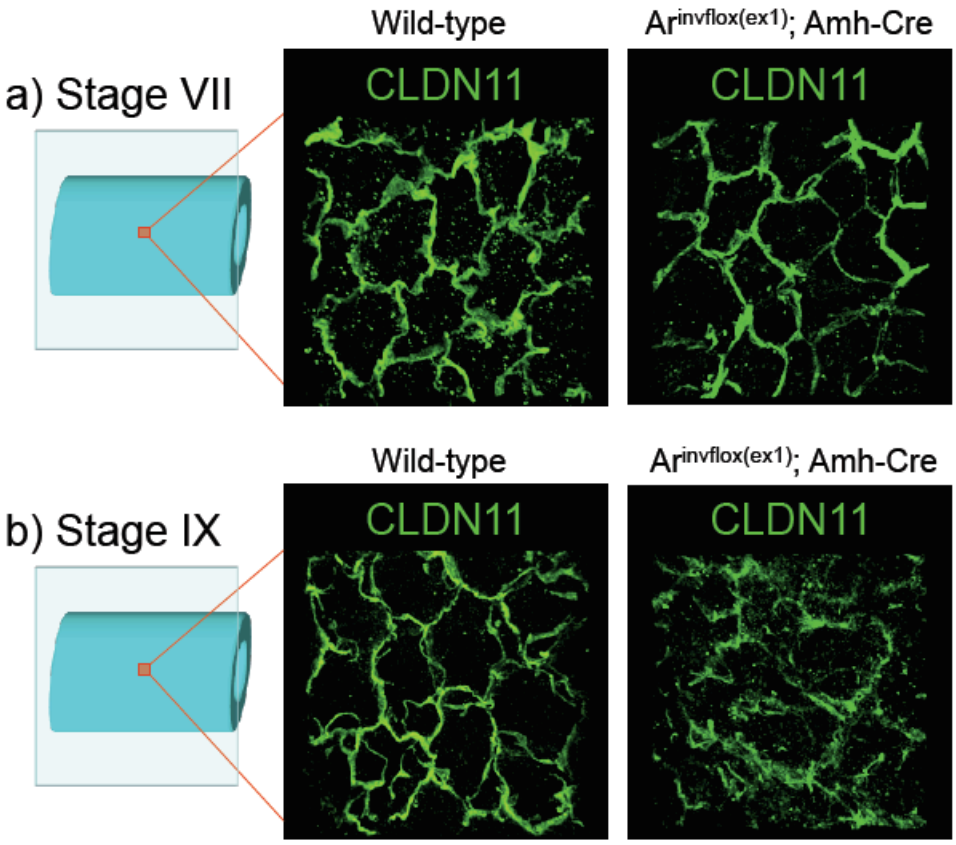

FIGURE 5. **The SCTJs are damaged during germ cell migration in AR deficient mice.** a) Prior to the preleptotene migration across the SCTJs, the CLDN11 (green) staining in the $Ar^{invflox(ex1)}$; Amh-Cre mice resembles that of the intact SCTJ barrier of a wild-type animal. b) As the spermatocytes begin their migration across the SCTJs, the CLDN11 staining reveals compartments forming in the wild-type animals, while the SCTJs in the $Ar^{invflox(ex1)}$; Amh-Cre animal become completely disorganized.

CHAPTER II: ANDROGEN RECEPTOR REGULATION OF SERTOLI CELL TIGHT JUNCTION REMODELING IS INDEPENDENT OF CLAUDIN-3

Abstract:

A component of the blood-testis barrier (BTB) is constituted by the tight junctions between adjacent Sertoli cells in the seminiferous epithelium. This stringent barrier conferred by the Sertoli cell tight junctions (SCTJs) provides a unique milieu for the developing germ cells by restricting the passage of solutes through the paracellular space. Androgens are key regulators of spermatogenesis and its action in Sertoli cells are mediated by androgen receptor (AR), a ligand activated transcription factor. Studies performed on Sertoli cell androgen receptor knockout (SCARKO) mice displayed SCTJ barrier defects and infertility in male mice. These mice showed a complete absence of claudin-3 (CLDN3) from SCTJs. Therefore, using a knockout mouse approach; we assessed the role of CLDN3 in the maintenance of SCTJ integrity. *Cldn3*-/- mice were fertile and did not display gross SCTJ structural defects as observed in the SCARKO mice. Lanthanum tracer studies indicated that the SCTJ barrier in *Cldn3-/-* mice were functionally intact. We therefore extended our analysis of SCARKO mutants and indentified deregulation of additional SCTJ components. We also identified an additional component of the SCTJs, claudin-13, which was differentially expressed in the SCARKO testis. Altogether, these results demonstrate that AR mediated maintenance of the SCTJ is orchestrated through a robust network of multiple tight junction components.

Introduction:

Spermatogenesis begins within the seminiferous epithelium with the testis. This specialized epithelium is formed by a radial arrangement of somatic support cells, the Sertoli cells, which extend from the basement membrane to the tubular lumen and are in direct contact with all testicular germ cells. Adjacent Sertoli cells form basally located specialized tight junctions (TJs) dividing the tubular epithelium into two distinct compartments. The basal compartment harbors the primitive stem cells, transit-amplifying spermatogonial cells and preleptotene spermatocytes, while the adluminal compartment contains the meiotic spermatocytes, post-meiotic spermatids and spermatozoa (Meng et al., 2011; Mruk and Cheng, 2004; Oakberg, 1956; Russell, 1977; Walker, 2010).

The BTB (blood-testis barrier) is constituted by the Sertoli cell tight junctions (SCTJs) in conjunction with the myoid cell tight junction in the tunica propria and the endothelial tight junctions of the interstitial micro-capillaries. It is one of the most impermeable epithelial barriers in mammals. While the endothelial tight junctions confer little barrier function to the BTB (Holash et al., 1993), an incomplete system of tight junctions between the myoid cells form a partial permeability barrier to electron-opaque tracers such as lanthanum. The continuous system of SCTJs however completely blocks the entry of tracers into the adluminal compartment. Thus, the SCTJs help create distinct cellular compartments within the seminiferous epithelium and generate a unique solute microenvironment conducive to maturing germ cells (Dym and Fawcett, 1970; Griswold, 1998).

The molecular composition of the SCTJs is remarkably similar to that in other epithelia: being composed of claudins, occludin and junctional adhesion molecules (JAMS) (reviewed in (Mruk and Cheng, 2004; Wong and Cheng, 2005). However, this tight junction is unique in its rapid remodeling properties. In spite of being periodically traversed by long chains of preleptotene spermatocytes, its barrier properties are not compromised (Dym and Cavicchia, 1977). Currently, our understanding of the SCTJ constituents, their functions and regulation is very minimal. The primary reason being the drawback of *in vitro* systems to recapitulate the multicellular, 3D dynamic structure processes that occur *in vivo*. Thus, genetic approaches using mouse models are by far provide the most informative strategies for studying regulation of SCTJ structure and function.

One of the most extensively studied regulators of the spermatogenic process is the androgen, testosterone. Depletion of testosterone or its receptor, androgen receptor (AR), leads to male sterility (Dohle et al., 2003). Cumulative data from multiple mouse models of androgen receptor depletion suggest androgen regulation at multiple spermatogenic processes (De Gendt et al., 2004; Holdcraft and Braun, 2004a). The two most sensitive steps being the conversion of round spermatids to elongated spermatids and the process of spermiation where elongated spermatids are released from the Sertoli cells (Holdcraft and Braun, 2004a). In mouse models of Sertoli cell-specific deletion of AR (SCARKO), a block in the pachytene/diplotene stages of meiosis and a loss of SCTJ integrity is observed (Chang et al., 2004; De Gendt et al., 2004; Holdcraft and Braun, 2004a; Meng et al., 2005; O'Donnell et al., 1999; Verhoeven et al., 2010; Willems et al., 2010). The concurrent expression of AR

in Sertoli cells during stages of SCTJ remodeling underscores the importance of AR as a key regulator of SCTJ reorganization during preleptotene migration (Bremner et al., 1994; O'Shaughnessy et al., 2010; Zhou et al., 2002). Microarray based expression analysis performed on a SCARKO model by Verhoven *et al* revealed altered expression of multiple SCTJ components such as *Zo-1* and *Jam3* in addition to the previously identified AR target gene *Cldn3* (De Gendt et al., 2004; Eacker et al., 2007; Meng et al., 2005; Willems et al., 2010). However, the direct involvement and relative contribution of these individual tight junction components in preserving SCTJ integrity still needs to be validated.

Claudins are the primary structural and functional units of TJs and the only proteins that can form TJs *de novo* in cell culture (Furuse et al., 1998b). Since the discovery of *Cldn1* and *Cldn2* in the late nineties, 27 different mammalian claudins have been identified, mostly by sequence homology and phylogenetic analysis (Furuse et al., 1998a; Mineta et al.). The distinctive features of the claudin proteins are the four transmembrane domains spanned by two extracellular loops and a conserved intracellular PDZ binding carboxyl tail. PDZ domain containing zona-occludins (ZO-1, ZO-2, ZO-3) family proteins (commonly referred to has tight junction proteins TJP1, TJP2 and TJP3, but herein referred to as zona-occludins for clarity) bind to the conserved intracellular loop and connect TJ components to the intracellular actinomyosin cytoskeleton (Furuse, 2010). Thus, TJ components, in addition to performing barrier functions, can also affect intracellular signaling events and mediate cellular processes such as proliferation, differentiation and cell

migration (Escudero-Esparza et al., 2011; Kohler and Zahraoui, 2005; Matter et al., 2005; Morin, 2005; Park et al., 2012).

The expression pattern of claudins is highly heterogeneous across various tissue types. Most cell types express more than two claudin proteins that associate by homo- and heterotypic interactions with claudins expressed on the adjacent membranes (Daugherty et al., 2007; Furuse et al., 1999; Tsukita and Furuse, 2000). These differential interactions and varied expression pattern in various tissues confer diverse properties to tissue specific tight-junction barriers (Kiuchi-Saishin et al., 2002). To date, claudins 3, 5 and 11 proteins have been localized to SCTJs (Morrow et al., 2010). While targeted deletion of *claudin 11* (*Cldn11*) in mice resulted in the absence of TJ strands in the seminiferous epithelium, highlighting its importance in SCTJ formation (Gow et al., 1999), the direct role of the two other known components of SCTJs are yet to be elucidated.

As a preliminary attempt to decipher the *in vivo* role of CLDN3, here we have specifically focused on the role of CLDN3 in SCTJ formation using a *Cldn3-/-* mouse model. We have then extended our studies to a newly generated SCARKO model to identify additional SCTJ components, loss of which may result in the SCTJ defects observed in these mice. Our data suggests that lack of CLDN3 alone is not sufficient to induce a SCTJ defect as observed in SCARKO mice. We identified deregulation of additional SCTJ components such as ZO-2, and a novel SCTJ component, (claudin13) CLDN13.

Results:

Generation and validation of Cldn3 null mouse

To determine the function of CLDN3 in SCTJ remodeling during preleptotene migration, we constructed a conditional null allele of *Cldn3*. *Cldn3* is a single exon gene on mouse Chromosome 5. As a targeting strategy, we introduced the first loxP site in the 5' UTR of the *Cldn3* gene. Using transient tansfection studies in HeLa cells, we confirmed that the introduction of the loxP site in the 5'UTR did not alter CLDN3 protein expression (Fig. S1A). The second loxP site was located distal to the neomycin resistance gene (*NeoR*) cassette. A 3.78-kb 5' homology arm and a 1.69-kb 3' homology arm was used to facilitate homologus recombination. Additionally, a diphtheria toxin cassette (DTA) and a cassette containing the gene for the viral thymidine kinase (TK) placed at the N- and the C-terminus of the subcloned mouse genomic fragment aided negative selection against random integration of the targeting vector into the ES cell genome. For Southern blots, multiple probes (3' genomic, 5' genomic and *Cldn3*-ORF) were designed to ensure proper integration of the targeting vector in the ES cells (Fig. 1A). G418 resistant clones were screened by Southern blot for correct targeting. Southern screening with the *Cldn3*-5' probe on ES cell DNA digested with Bsm1 yielded a 8.1-kb DNA band representing the wild-type allele and a 5.7-kb fragment of the floxed allele. The ES cell clone of interest was further confirmed using a *Cldn3*-3' probe which yielded the expected band sizes of 8.1-kb and 3.8kb (Fig. S1B). $Cldn3^{+/fl}$ mice were generated according to conventional procedure. Tail DNA from $Cldn3^{+/fl}$ mice were subjected to a

confirmatory Southern screening with the *Cldn3*-ORF probe on DNA digested with Bsm1/BstB1. A 5.7-kb DNA band representing the floxed allele and a 3.4-kb fragment in the wild-type allele were observed as expected (Fig. 1C).

Cldn3$^{+/fl}$ mice were crossed with transgenic mice expressing Cre recombinase to generate Cldn3$^{+/-}$ mice (see methods). Excision by Cre-mediated recombination permitted the removal of the *Cldn3* exon in conjunction with the *NeoR* cassette generating a null allele. Homozygous Cldn3$^{-/-}$ mice were obtained by intercrossing the heterozygous mice. PCR primers E1 and E2 confirmed loss of the *Cldn3* exon. The wild-type and the floxed allele were distinguished by a separate pair of primers P1 and P2 in independent PCR reactions. Additionally, *Cldn3* -specific primers confirmed the absence of the *Cldn3* ORF in the Cldn3$^{-/-}$ mice (Fig. 1B, D). *Cldn3* and *Cldn11* RNA expression was assessed in testis samples of Cldn3$^{-/-}$ mice and their corresponding littermate controls at 10 weeks by qRT-PCR analysis. *Cldn3* RNA was undetectable in testis samples of Cldn3$^{-/-}$ mice, compared to controls, whereas *Cldn11* RNA levels remained unchanged (Fig. 1E). Similar observations were made in other tissues such as the lung and the liver (Fig. S1C).

Western blot analysis of total testis protein using α-tubulin as a loading control confirmed the absence of CLDN3 protein in *Cldn3*-null mice as expected (Fig. 1F). In parallel experiments, whole-mount immunostaining on seminiferous tubules confirmed the absence of CLDN3 in mutant testis (Fig. 1G). We had initially identified *Cldn3* as an androgen responsive target gene in Sertoli cells and have shown that CLDN3 localized to sites of the new tight junction, during stages VIII–X of the spermatogenic cycle (Meng et al. 2005). Thus, we assayed CLDN3 protein

localization in testis in stage IX tubule sections by immunofluorescence microscopy. A stage IX section was identified using the nuclear counterstain DAPI on the tubular cross-sections. In wild-type samples, CLDN3 was detected near the basal lamina of the epithelium coinciding with CLDN11 expression, a known component of the SCTJs, whereas CLDN3 staining was absent in the seminiferous epithelium of Cldn3$^{-/-}$ mice. Interestingly, the staining pattern of CLDN11 was not diminished suggesting that the SCTJ structures still formed in the mutant mice (Fig. 1H).

Consequences of **CLDN3** *loss and its specific effects on the spermatogenic process*

Previous work has shown that genetic deletion of *Cldn11*, a component of the SCTJs, leads to loss of SCTJs in the testis and caused male sterility. Additionally, absence of CLDN11 in the basal cell tight junctions and the central nervous system (CNS) leads to deafness and lack of CNS myelin sheath respectively. Thus, deletion of CLDN11 in tissues expressing this protein lead to severe tight junction defects indicating that it is a key structural component of the TJs (Gow et al., 2004; Gow et al., 1999; Mazaud-Guittot et al., 2010). While loss of CLDN11 lead to major defects in tissues expressing CLDN11, such as the nervous system, the olfactory epithelium and the testis, we were interested to query the consequences of the global effects of the genetic depletion of CLDN3 in addition to its role in SCTJs. In contrast to CLDN11, CLDN3 expression is ubiquitous across tight junctions of multiple vital tissues. Its expression is detected in early embryonic stages followed by its expression across tissues such as the brain, liver, lung, kidney, intestine, testis etc. in

adult mice (Haddad et al., 2011; Hashizume et al., 2004; Liebner et al., 2008; Meng et al., 2005; Morita et al., 1999a; Ohta et al., 2011). Surprisingly, *Cldn3*$^{-/-}$ mutant mice were viable on both 129Sv/ImJ (129) and C57BL/6J (B6) backgrounds. Furthermore, no gross structural abnormality was detected in hematoxylin-eosin stained histological sections of tissues expressing CLDN3 (data not shown).

To test the functional consequences of the lack of CLDN3 on the overall spermatogenic process, we performed gross-histological analysis of testis cross-sections, sperm counts and fertility analysis on both *Cldn3-/-* mutants and corresponding wild-type mice. Within the *Cldn3-/-* testes seminiferous tubules, all spermatogenic stages were observed on histological sections. Step 16 spermatids were detected at stage VIII indicating successful completion of the spermatogenic cycle (Fig. 2A). Overall, no significant differences in body weight, testis weight and epididymal sperm count were detected at 10 weeks of age (Fig. 2B). In order to further test the functionality of the sperm, the fertility of *Cldn3-/-* males was assessed. Average litter sizes generated from four different *Cldn3-/-* males and their wild type littermates were documented. No change in average number of pups was observed indicating that the sperm produced by both groups of animals were functional (Fig. 2C).

Assessing SCTJ barrier function in absence of CLDN3

In our previous work using 3D imaging, we have conclusively demonstrated that during migration the preleptotene spermatocytes are briefly enclosed in a transient intermediary compartment formed by Sertoli cell tight junctions. We

hypothesize that the formation of this intermediary compartment formed by two distinct layers of the old TJ at the adluminal side and the newly forming TJ basal to the preleptotene spermatocyte is critical for preserving the barrier function during the migration of these cells. Interestingly, in wild-type mice CLDN3 protein was observed bridging the gaps in the newly forming tight junction suggesting that it may play a critical role in new SCTJ formation (see Chapter 1). To test such a possibility, we performed whole-mount immunostaining with CLDN11, a known component of the SCTJ, and imaged regions of the seminiferous tubules where preleptotene spermatocytes were migrating across the SCTJs. The spermiation front was used to identify these regions. We observed the formation of a transient intermediary compartment marked by CLDN11 (white asterisks) in both *Cldn3-/-* and wild-type testis indicating that the formation of the new tight junctions was not grossly altered in the absence of CLDN3 (Fig. 3A). To further confirm the above findings, we tested the functional integrity of the SCTJ in a permeability assay using lanthanum as an intracellular tracer. It is well established that SCTJs form one of the most stringent barriers in mammals and restricts the permeability of tracers such as ferritin, peroxidase and lanthanum.(Dym and Fawcett, 1970; Fawcett et al., 1970; Neaves, 1973). Analysis of histological sections from two *Cldn3-/-* mice showed lanthanum penetration through the myoid cell tight junction layer of the tubules and the intercellular space around the spermatogonia in 25% of the tubules. However, the lanthanum did not diffuse beyond the SCTJ towards the adluminal compartment. These results were similar to those observed in wild-type mice. Additionally, the ultrastructure of the *Cldn3-/-* SCTJs appear similar to the control mice exhibiting a

series of electron dense kissing points, representing lipid bilayers of adjacent Sertoli cell membranes in close proximity to form an impermeable barrier (Fig. 3B).

A compromised SCTJ could lead to loss of testicular immune privilege and result in testis-specific antibodies (Meng et al., 2011). Therefore, we tested for the presence of auto-antibodies against post-meiotic germ cells in sera collected from wild-type and *Cldn3-/-* mice. Histological sections of 8-week-old testis were subjected to immunohistochemistry with sera obtained from both *Cldn3-/-* mutant and control animals (n=6). No significant reactivity was observed in either samples indicating that the testicular immune privilege was not compromised in absence of CLDN3 (Fig. 3C).

Construction and analysis of conditional exon 1 androgen receptor allele in Sertoli cells

It is well established that androgen receptor function in Sertoli cells is a key mediator of multiple spermatogenic events including maintenance of SCTJ integrity and function (Eacker et al., 2007; O'Shaughnessy et al., 2010; Verhoeven et al., 2010; Willems et al., 2010). We have previously identified *Cldn3* as a transcriptional target of the androgen receptor and hypothesized it to be critical for maintenance of SCTJ integrity (Eacker et al., 2007; Meng et al., 2005). The SCTJ phenotype disparity between *Cldn3* null mice and Sertoli cell AR knockout (SCARKO) models suggests that additional molecular dysregulations are present in the SCARKO testes that account for the SCTJ phenotype. Therefore, we have revisited the SCARKO model to

identify novel AR regulated SCTJ components that are integral to SCTJ structure and function.

Our previously described model of AR depletion used the *Ar*^{tm1Reb} allele which contains inverse oriented LoxP sites flanking exon 1 and the NeoR gene cassette in intron 1. Exposure of this allele to Cre recombinase leads to the inversion of exon 1 and produces an AR protein null phenotype as was seen when we combined it with the Tg(Amh-Cre) transgenic line, which expresses Cre recombinase in the fetal Sertoli cells (Holdcraft and Braun, 2004a). Importantly, the Artm1Reb allele behaves as a hypomorph, independent of Cre, due to a cryptic splice acceptor in the NeoR gene. While the Ar^{tm1Reb};Tg(Amh-Cre) genetic model exhibits a loss-of-function (LOF) phenotype in the Sertoli cells, all remaining cell types maintain the Ar hypomorphic state. The consequence of this is a compensatory elevation in testosterone levels due to the hypothalamus-pituitary-gonad autocrine feedback loop (Holdcraft and Braun, 2004a; Holdcraft and Braun, 2004b). Though we observed SCTJ defects in this mouse model, the deregulation of downstream pathways could be an effect on transcription (due to AR loss), or due to non-AR dependent androgen signaling (Holdcraft and Braun, 2004b; Walker, 2010) or a combination of both. To overcome the above complications in relation to interpreting the SCTJ phenotypes in our previous model, we generated a new conditional androgen receptor allele that allowed us to delete Ar exon 1 in Sertoli cells while maintaining all other cells in a fully functional Ar genetic state.

We redesigned our original exon 1 conditional gene targeting vector to allow us to ultimately produce Ar exon 1 Sertoli cell knockout (SCARKOtm2) mice. First,

both LoxP sites flanking exon 1 of the *Ar* gene were orientated as direct repeats to allow the deletion of the intervening sequences (Fig. 4A). This novel Ar vector was used to target the endogenous Ar locus in 129S1/SvImj ES cells. To remove any influence of the NeoR gene on the *Ar* locus, we excised the Neo^{R} cassette from a recombinant clone by transient expression of FLP recombinase to ultimately produce ES cell clones with the novel Ar^{tm2Reb} allele (Fig. 4A). Chimeric mice were produced with two clones and one line transmitted the Ar^{tm2Reb} allele through the germline in an X-linked gene segregation pattern as expected since the *Ar* gene is located on the X chromosome. Male mice carrying the conditional allele (Ar^{tm2Reb}/Y) are viable, fertile and show no quantitative or qualitative impact on spermatogenesis based on testis mass, testis histology, sperm counts and reproductive success (data not shown). These data contrast the Ar^{tm1Reb} allele and suggest the Ar^{tm2Reb} allele is fully functional prior to Cre mediate exon 1 deletion. We confirmed if the Ar^{tm2Reb} allele could undergo proper recombination and produce a LOF phenotype characteristic of the classic LOF *Ar* allele, *Tfm*, which produces Ar^{Tfm}/Y mice that externally appear as females but contain undescended testes (Hutson, 1986). Whole body exon 1 deletion ($Ar^{(Dexon1)}$/Y) mice produced an identical set of phenotypes as Ar^{Tfm}/Y mice (data not shown). PCR genotyping confirmed the loss of 5' and 3' LoxP sites and the generation of the novel PCR product predicted from a post-Cre recombination event at the *Ar* locus (Fig. 4B). Finally, we deleted exon 1 specifically from Sertoli cells by mating Ar^{tm2Reb} females with TgAmh-Cre males and found Ar^{tm2Reb}/Y;TgAmh-Cre mice were externally male in appearance and contained descended testes with reduced size (Fig. 4C). Similar to

other SCARKO genetic models with conditional ablation of more 3' *Ar* exons, our SCARKO model showed a block in spermatogenesis at the meiotic to spermiogenenic stage of development as exemplified by the lack of haploid cells (Fig. 4C). Immunostaining with an anti-AR antibody directed at the N-terminus showed a complete absence of signal in SCARKO Sertoli cells while other AR expressing cell types, such as Leydig and myoid epithelial cells, were unaffected (Fig. 4D). Together, these data show our new *Ar* allele can conditionally delete *Ar* exon 1 sequences to produce a molecular and genetic LOF mutation and does not exhibit hypomorphic activity prior to Cre exposure.

Deregulation of Sertoli Cell Tight Junction architecture and its components in SCARKO mice

Our previously reported hypomorphic mouse model of *Ar* depletion (Ar^{Tm1Reb}/Y; Amh-Cre) exhibited a compensatory elevation of androgens and a SCTJ barrier defect. These mice displayed a complete lack of CLDN3 from SCTJs marked by CLDN11 (Holdcraft and Braun, 2004a; Meng et al., 2005). Confocal imaging of whole-mount seminiferous tubules using CLDN11 as a marker for the SCTJs, revealed disorganization of the SCTJs, specifically during transit of preleptotene spermatocyes in stage IX. Similar to Ar^{Tm1Reb}/Y; Amh-Cre mouse testis, our SCARKO mice also exhibited moderate to severe disorganization of SCTJs in parts of the seminiferous tubules (Fig. 5A). However, contrary to Ar^{Tm1Reb}/Y; Amh-Cre testis, the SCTJs were severely disorganized in all tubules, enveloping individual

spermatocytes within the SCTJs. These observations compliment studies performed on another SCARKO model that exhibited SCTJ barrier defects (Willems et al., 2010).

In order to reconcile the severe SCTJ defects observed in SCARKO mice, which lack any detectable CLDN3, and an absence of SCTJ defects in *Cldn3* null mice, we first wanted to address whether the SCTJ barrier defect in SCARKO mice was an indirect effect of the loss of haploid germ cells within the SCARKO testis. To address this, we performed confocal imaging of SCTJs in $Kit^{W}/Kit^{W\text{-}v}$ mice that are devoid of meiotic and post-meiotic germ cells (Mintz and Russell, 1957; Yoshinaga et al., 1991). We observed morphologically intact SCTJs in these mice (Fig. 5A), suggesting that the presence of spermatocytes and spermatids are not essential for the maintenance of SCTJs. This lead us to hypothesize that deregulation of multiple tight junction components, in addition to CLDN3 could result in the compromised SCTJs observed in the SCARKO testis.

In order to identify additional SCTJ components that are deregulated in SCARKO mice, we performed real-time PCR analysis and assessed the testicular mRNA levels of all 26 murine claudins known till date (Mineta et al., 2011). In addition, mRNA expression of other known tight junction components such as occludin, junction adhesion molecule 2 and 3 (JAM2, JAM3), and zona-occludin 1, 2, and 3 (ZO-1/2/3) were analyzed. *Cldn3-/-* mice were also included in this analysis to investigate compensatory mRNA expression changes in SCTJ components that could occur in the absence of CLDN3 (Fig. S2). We observed a significant downregulation of several tight junction associated transcripts in the SCARKO testis, relative to control mice. mRNA transcripts of *Cldn3, Cldn13, Cldn 20, Zo-1 and Zo-2* isoform C

(Zo-2C) were significantly downregulated in SCARKO mutants (Fig. 5B). In *Cldn3*$^{-/-}$ testis, *Zo-2C* was significantly upregulated compared to controls (Fig. S2).

Next, we assessed whether the protein levels of CLDN3, CLDN13, CLDN 20, ZO-1 in SCARKO mice. Using immunohistochemistry, we confirmed the presence of CLDN13 at the SCTJs (Fig. 5C). We also performed immunoblotting on total protein lysates from wild-type and SCARKO testes. Surprisingly, we found that protein levels of transcripts that were not differentially expressed at the mRNA level, such as *Cldn5* and *Occludin,* were more abundant in SCARKO testis compared to wild-type controls. Analogously, protein levels for *Cldn13* and *Zo-2* transcripts (that were downregulated in SCARKO mutants), were equally abundant in mutant and control mice (Fig. 5D). We rationalize this disproportionate increase in protein expression to the differential cellular composition of the wild-type and SCARKO testis. It is known that transcriptionally silent spermatids (elongating and elongated) are enriched in proteins due to active translation (Stern et al., 1983) with a corresponding depletion of the mRNA pool (Morales and Hecht, 1994). Thus, absence of spermatids in the SCARKO testis causes a significant depletion of the total protein pool while minimally impacting the total RNA pool, when compared to wild-type mice. Therefore, total protein lysates of SCARKO testis are enriched in Sertoli cell-specific proteins relative to wild-type controls (note, increased levels of CLDN5 and Occludin in Fig. 5D). Therefore, downregulated transcripts such as *Cldn13* and *Zo-2* appear as equally abundant proteins in SCARKO mutant compared to controls. Thus, levels of CLDN13 and ZO-2 proteins are indeed reduced in SCARKO mutants, when normalized to tight junction proteins such as CLDN5 and

occludin, RNA levels of which are unaltered. CLDN20 was undetectable in both mutant and wild-type testis by immunoblot analysis.

We then wanted to determine whether transcripts that were downregulatedin the SCARKO testis, would also be enriched in the stages VII-X of the seminiferous epithelial cycle that have the highest AR expression in Sertoli cells (Vornberger et al., 1994). To do so, we used transillumination microdissection of wild-type seminiferous tubules to isolate three sets of tubules: stage III-VII, stage VII-XI and stage XI-III (Kotaja et al., 2004). We used stimulated by retinoic acid gene 8 (*Stra8*) as a marker for stage specific expression, as it is known to have peak transcription between stages VI and VIII (Zhou et al., 2008). We observed *Cldn3* and *Cldn13* to be significantly more abundant in stages VII-XI relative to stages III-VII and stages XI-III ($p<0.05$ each). *Zo-2* was also enriched in stages VII-XI in comparison to stages III-VII ($p<0.05$). However, the difference in expression between stages VII-XI and stages XI-III was not significant ($p=0.08$). *Stra8* was significantly enriched in stages VII-XI ($p<0.01$) confirming that the samples were staged correctly (Fig. 6).

Discussion:

Identification and selective depletion of AR target genes is essential to understanding how androgen action in Sertoli cells supports spermatogenesis. Using a knockout mouse model, we show here that depletion of the AR target gene, *Cldn3,* from SCTJs does not recapitulate the SCTJ defects observed in SCARKO mutants. Three-dimensional confocal imaging of seminiferous tubules confirmed that the formation of the transient tight junction compartment that encloses preleptotene spermatocytes during their migration to the adluminal compartment was not altered in the absence of CLDN3. Lanthanum based tracer studies further proved that the SCTJs were functionally intact in *Cldn3*$^{-/-}$ mice. As a consequence, we did not observe any testicular auto-antigens in sera obtained from mutant mice. Also, male mice showed no fertility defects in the absence of CLDN3. Gene expression analysis of specific tight junction components in *Cldn3*$^{-/-}$ mice did not show a compensatory increase in other members of the claudin family of proteins.

We therefore reanalyzed the SCARKO mutants to try and identify any additional tight junctional components that are deregulated in the testis, to better explain the SCTJ defects observed in SCARKO mutants. We scanned for expression levels of the claudin gene family, in addition to other known tight junction associated transcripts by real-time PCR. We found altered transcript levels of multiple tight junction components, including *Cldn13, Cldn20, Jam2, ZO-1* and *ZO-2C* in addition to *Cldn3*. We identified CLDN13 as a novel tight junction component that localized to SCTJs in the testis. *Cldn13* was also enriched in stages of the

seminiferous cycle corresponding with peak AR expression in Sertoli cells, suggesting that *Cldn13* may be direct gene target of AR.

The observation that CLDN3 localizes specifically to newly forming SCTJs as well as the SCTJ defects observed in SCARKO and *Gnpat*-null mice that exhibited loss/ downregulation of CLDN3 (Holdcraft and Braun, 2004a; Komljenovic et al., 2009; Meng et al., 2005; Willems et al., 2010), lead us to hypothesize that CLDN3 is a key mediator of SCTJ remodeling in the testis. However, since SCTJ defects were not observed in *Cldn3-/-* mice and the mice were fertile, it was evident that unlike CLDN11, CLDN3 is not an essential structural component of SCTJs (Gow et al., 1999). We also did not find any histological or barrier defects in *Cldn3-/-* tissues that normally express CLDN3, including the brain, lung, thymus, liver, kidney, and intestine (Hamazaki et al., 2007; Holmes et al., 2006; Liebner et al., 2008; Morita et al., 1999a). *Cldn3-/-* mice were viable with no apparent physiological dysfunctions. Altogether, these findings rule out the role of CLDN3 as an essential structural component of tight junctions.

Methods:

Animals

All mice were bred and maintained in a high barrier facility at the Jackson Laboratory. All experimental protocols were approved by the Jackson Lab Institutional Animal Care and Use Committee (ACUC) and were in accordance with accepted institutional and government policies.

Gene targeting and generation of a Cldn3 -floxed allele

To construct the conditional *Cldn3* gene targeting vector, BAC clone (RP23-153011) containing the *Cldn3* genomic fragment was obtained from mouse RP23 BAC genomic library (CHORI, Oakland, CA). Xmn1-digested DNA fragments were shotgun subcloned into the pBluescript (pBS) vector. Colony hybridization was then performed using a *Cldn3* probe to select the pBS clone containing the 5.4-kb genomic fragment of the *Cldn 3* locus (termed pBS-*Cldn3*-Xmn). A LoxP site containing a synthetic oligo was introduced into the BstB1/Not1 site in the 3' UTR of the *Cldn 3* gene into the pBS-*Cldn3*-Xmn vector (termed pBS-LoxP-*Cldn3*-Xmn). The BstB1 5' overhang in the synthetic oligo was modified from CGAA to CGCA to obtain a non-functional BstB1 site to facilitate screening of correctly targeted clones at later steps. *Cldn3* cDNA sequence (both with and without LoxP) was subcloned by PCR into the SacII and BamH1 ends of a pIRES2-EGFP vector. These constructs were used in transfection studies to compare the expression of CLDN3 protein in presence and absence of the LoxP site.

A 1.6kb EcoRV-Xmn fragment from the pBS-LoxP-*Cldn3*-Xmn vector, 3' of the *Cldn3* locus was subcloned into 5' multiple cloning site of the targeting vector pBS4600 kindly provided by Dr Richard Palmiter (University of Washington School of Medicine, Seattle). A 3.7 kb fragment containing 2.4 kb 5' genomic region and the *Cldn3* exon was subcloned into the 3' multiple cloning site of the targeting vector pBS4600. The functionality of the loxP sites was confirmed by excision using an *in vitro* Cre reaction (NEB, Ipswich, MA). The *Cldn3* conditional knockout vector was linearized with Asc I and electroporated into 129S1/SvImJ embryonic stem (ES) cells. ES cell clones of interest were enriched by a positive selection based on neomycin and a negative selection based on the thymidine kinase and diptheria toxin A. ES cell clones with one targeted allele were identified by Southern blot analysis by probing Bsm1/BstB1 or Bsm1 digested DNA with PCR-generated probes. Targeted ES clones were microinjected into C57BL/6 blastocysts to generate chimeric mice. The chimeric males were crossed to C57BL/6 females to identify mice with germline transmission.

Chimeric floxed-*Cldn3* allele harboring mice were crossed to both129S1/SvImJ and C57BL/6 females. The C57BL/6 FI progeny was backcrossed for 6 generations for experimental purposes. Floxed 129S1/SvImJ mice were crossed to a transgenic TNAP-Cre deleter strain (129-Alpl$^{tm1(cre)Nagy}$/J, Stock number 008569; The Jackson Laboratory, Bar Harbor, ME). The F1 TNAP Cre; *Cldn3*$^{+/-}$ mice were interbred to generate a global deletion of *Cldn3*. The floxed C57BL/6 strain was crossed to a transgenic CMV-Cre deleter strain, (B6.C-Tg(CMV-cre)1Cgn/J, Stock number 006054; The Jackson Laboratory, Bar Harbor, ME**)** and bred as above to

generate a global deletion of *Cldn3* on the C57BL/6 background. The effects of *Cldn3* deletion on both backgrounds were analyzed.

Gene targeting and generation of an Ar exon 1 floxed allele

To generate a novel *Ar* conditional allele, a 9.5 kb *Sac*I fragment containing the first exon of *Ar* was subcloned into the pBS vector from the 12.5 kb fragment used to generate the Ar^{tm1Reb} allele Holdcraft 2004 reference). A LoxP site and a unique *BstE*II restriction enzyme site were introduced at a *Stu*I site 2.5 kb from the transcriptional start site of Ar. A neomycin resistance (Neo^R) cassette was inserted in a *BamH*I site immediately 3' of the splice donor of *Ar* exon 1. The Neo^R was flanked by Flp-recombinase target (FRT) sites and by a single LoxP site at the 3' end of the cassette (a generous gift from Dr. Gail Martin). A *Sal*I-*Xho*I fragment containing a CMV promoter-driven diptheria toxin (Dta) was inserted into an *Xho*I site in the polylinker sequence at the 3' end of the construct for use in negative selection in ES cells. Linearized targeting vector was electroporated into 129S1/SvImJ ES cells and G418 resistant clones were expanded for Southern blot analyses. Properly targeted clones were identified by probing Southern blots containing *EcoR*V digested genomic DNA with an *Ar* exon 1 probe. Of 288 clones analyzed, 3 showed the presence of a the predicted 9.2kb recombinant allele along with the loss of the 12.5 kb WT allele due to the ES cells being genetically XY. Further screening by double digest with *EcoR*V and *BstE*II showed that all of the 3 colonies had incorporated the 5' LoxP site as part of the recombination event. One properly targeted clone was electroporated with a CMV-Flp recombinase expressing

plasmid to remove the neoR cassette flanked by the FRT sites. 5 of 93 clones proved to be G418 sensitive suggesting loss of the Neo^R cassette. 3 clones were analyzed further by Southern blot analyses using EcoRV/BstEII digested genomic DNA. All 3 clones displayed the predicted 10.3 kb fragment indicative of Flp mediated removal of the Neo^R cassette and a 3' arm that underwent proper homologous recombination. Neo^R negative targeted ES clones were microinjected into C57BL/6J blastocysts to generate chimeric mice. The chimeric males were crossed to C57BL/6J and 129S1 to produce B6129F1 hybrid and 129S1 inbred mice carrying the targeted Ar^{tm2Reb} allele. 129S1-Ar^{tm2Reb} heterozygous females were bred with 129S1-Tg(Amh-cre) males to produce SCARKO male mice. B6129F1- Ar^{tm2Reb} heterozygous females were bred with 129-$Alpl^{tm1(cre)Nagy}$/J males to produce heterozygous Ar^{tm2Reb} females that have deleted exon 1 in the germline due to the Cre expression from the $Alpl^{tm1(cre)Nagy}$ allele. These females were mated with 129S1/SvImJ wild-type males to produce male mice containing whole body knockout of *Ar* exon 1.

Southern blotting

Genomic DNA was purified using the DNeasy kit (Qiagen, Valencia, CA). 10 ug genomic DNA was digested overnight at 65°C with BstB1/Bsm1 or Bsm1 and resolved on 0.8% agarose gel by electrophoresis for 19 hs at 40 volts (V). The gel was depurinated in 0.25M HCl for 10 minutes, rinsed with water and denatured in 0.5 M NaOH,1.0 M NaCl for 30 minutes on a shaker. After rinsing with water, the gel was then neutralized in 0.5 M Tris-HCl, pH 7.4, 1.5 M NaCl for 30 minutes. DNAs

were transferred onto GT Zeta Probe Membrane (Biorad, CA) by capillary transfer for 19 h at room-temperature in 20×SSC. Blots were dried for 30 minutes, UV crosslinked and pre-hybridized for 60 minutes at 65°C in 6×SSC, 5×Denhardt's solution, 0. 5 mg/ml salmon sperm DNA, 0.5%SDS, 10% dextran sulphate. An additional 10ml of the prehybridization buffer containing 50 ng of radiolabeled probe was added to the membrane and hybridized overnight at 65°C. For radiolabeling, 50 ng of the probe was heated at 95°C for 3 minutes, placed on ice for 2 minutes and labeled with 5 ul of ^{32}P -CTP (BLU513H250, Perkin Elmer, Waltham, MA) at 37°C for 60 minutes. Unlabeled nucleotides were removed using a micro spin-column (Amersham, Piscataway, NJ). The purified probe was boiled for 5 minutes prior to hybridization. The blots were washed twice for 45 minutes at 65°C in 2×SSC, 0.5% SDS, then for 30 minutes at 65°C in 0.15×SSC, 0.5% SDS, and 20 minutes at room temperature in 0.1×SSC, 0.1% SDS, followed by exposure to phosphor screens at room temperature for three days. The screens were scanned in a Fuji FLA-5100 scanner (Fujifilm, Tokyo, Japan).

Genotyping

Mice were genotyped by mixing the following primers in a single PCR for detection of the floxed allele: F 5' CGT CAG TTT TCG AAG GGC AGT TG-3' and R 5'GGT GAT CTC CAG GCC CAT GG-3'. To confirm the deletion of the *Cldn3* exon the following primers were used. F 5'- CCC AGT CTC AGA AGC CAG TC -3' R 5'- GAT AAA CCT CGC TCG CCA TA -3'. The expected amplicon sizes were 127 bp, 315 bp, and 161 bp for *Cldn3* wildtype, null, and conditional floxed alleles, respectively. PCR

detection of the Ar^{tm2Reb} allele was accomplished by detection of the 5' LoxP and 3' LoxP sites in separate reactions. Ar_P1 (5' 3') and Ar_P2 (5' 3') primer pair amplify the 5' LoxP site to produce a 200 bp and 220 bp WT and targeted conditional allele respectively. A Ar_P3 (5' 3') and Ar_P4 (5' 3') primer pair amplify the 3' FRT-LoxP site to produce a 200 bp and 220 bp WT and targeted conditional allele respectively. The post-Cre recombinase allele is amplified using the Ar_P1 and Ar_P4 primers and produces a 450 bp product. Genotyping of the Cre transgenic allele included the primer set: F 5'-TGGTTTCCCGCAGAACCTGAAG-3' and R 5'-GAGCCTGTTTTGCACGTTCACC-3' and yields a 220 bp product.

Histology and immunohistochemistry

Weights of testes collected from each animal were recorded following which tissues were fixed overnight at 4°C in Bouin's fixative. Testes were rinsed with water and dehydrated for paraffin embedding. For histological analysis, 5-µm sections were cut and mounted on glass slides and stained with Periodic Acid / Schiff's (PAS) reagent using standard procedure. For immunocytochemical studies, tissues were fixed in neutral-buffered formalin (NBF), rinsed with PBS (Phosphate Buffered Saline) followed by dehydration in 70% ethanol and then embedded. Sections were deparaffinized (2×10 minutes) in Xylene, and rehydrated (2×5 minutes) in 100% ethanol, (1×5 minutes) in 95% ethanol, (1×5 minutes) in 70% ethanol, (1×5 minutes) in 50% ethanol, (1×5 minutes) in PBS. For antigen retrieval, slides were boiled in 10mM sodium citrate (pH 6.0) for 10 minutes. The sections were blocked in 3% normal donkey serum for 1h at room temperature followed by

overnight incubation in primary antibody in 3% normal donkey serum at 4°C. Following washes in PBS, sections were incubated with secondary donkey anti-rabbit or anti-mouse antibodies conjugated to Alexa Fluor®568 or Alexa Fluor®488 (Molecular Probes, Grand Island, NY). Slides were rinsed in PBS and mounted in Vectashield mounting media with DAPI (Vector Laboratories, Burlingame, CA). Images were aquired on a Nikon Eclipse E600 microscope equipped with an EXi Aqua Camera from QImaging® (Surrey, BC, Canada).

Epididymal sperm counts

A single epididymis from each animal was minced in 1 ml PBS and sperm allowed to swim out for 1 h at 37°C. Epididymal sperm counts were determined using a hemocytometer.

Serum collection

Mice were euthanized by CO2 anesthesia. Blood was collected by cardiac stick using a 25 ½ gauge heparinized needle. Samples were spun for 2 min for 2000rcf. The top, serum fraction was carefully collected and frozen at -80oC for future use.

Whole-mount immunostaining

Adult (2-3 months) male 129S1/SvImJ or C57BL/6J mice were euthanized with CO_2 and the testes were immediately transferred onto chilled PBS. The tunica albuginea was then removed and the seminiferous tubules were teased apart. The

interstitial cells were removed by incubating the tubules in 0.5mg/mL collagenase (Sigma, St. Louis, MO) at room temperature (RT) for 5 minutes while continuing to tease the tubules apart. The tubules were then rinsed three times with PBS, and fixed in 2% paraformaldehyde (Electron Microscopy Sciences, Fort Washington, PA) for 6 h at 4°C.

Paraformaldehyde-fixed tubules were rinsed three times with PBS, and permeabilized with 0.25% NP-40 in PBS-T (PBS + 0.05% Tween for 25 minutes at RT. The tubules were rinsed three times with PBS-T, 5 minutes each, and blocked using 5% normal donkey serum (Jackson Immuno Research, West Grove, PA) in PBS-T either 2 h at RT or over-night at 4°C. The tubules were labeled with one of the following primary antibodies, diluted in PBS-T, 5% normal donkey serum over-night at 4°C and rinsed three times with PBS-T, 5 minutes each. The tubules were then stained with a combination of the secondary antibodies for 1 h at room temperature. Samples were then rinsed three times with PBS-T, 5 minutes each with DAPI added to the first rinse. The tubules were spread in a drop of VectaShield® with DAPI (Vector Laboratories, Burlingame, CA), covered with a coverslip, and sealed with nail polish.

Antibodies

Primary antibodies diluted 1:200 in PBS-T + 5% normal donkey serum over-night at 4°C. Antibodies were purchased from the following companies. Rabbit α-Cldn11 H-107 (Santa Cruz Biotechnology, Santa Cruz, CA), rabbit α-Cldn3 (Zymed

Laboratories, San Francisco, CA), rabbit α-alpha tubulin (Abcam, Cambridge, MA), mouse α-actin (Sigma-Aldrich, St. Louis, MO).

Confocal microscopy of seminiferous tubules

The seminiferous tubules were imaged on a Leica® TCS SP2 laser scanning confocal microscope. The images were acquired using serial sections starting from the basement membrane and ending on the apical side of the SCTJs with an average voxel size of 150nm x 150nm x 150nm. The stage of the seminiferous epithelial cycle at which the series were taken was confirmed using both DIC and DAPI optical cross sections. The image series were rendered using the Amira® 4.1.2 software package (Visage Imaging, VIC, Australia). Heat-map colorimetrics were used, where blue light intensity, such as DAPI fluorescence, is represented on a blue to white heat map and red fluorescence, such as CLDN11, is represented on a red to bright yellow heat map. Isosurfaces were rendered using a fixed color.

Tracer studies

The mice were first perfused through the left ventricle with 30 ml of saline (0.85% NaCl) solution (37°C) containing 2 units of heparin/ml to flush out the blood. Lanthanum hydroxide, pH 7.8 was prepared by slowly adding 0.1 N and then 0.01 N NaOH dropwise to 4% (w/v) La(NO3)3. 6H20 (Sigma-Aldrich, St. Louis, MO) in degassed water. 10 wk old mice were perfused through the left ventricle with 50 ml of a freshly prepared solution of 1:1 mixture of (5% gluteraldehyde, Electron Microscopy Sciences, Hatfield, PA, in 0.2M s-collidine, pH 7.4 and 4% lanthanum pH 7.8). The hardened testes were dissected, cut into small cubes (2-3 mm^3) and

immersed in the same lanthanum containing fixative for an additional 1 h at room temperature. After repeated rinsing in the buffer (0.2M s-collidine, Polysciences Inc., Warrington, PA, containing 2% lanthanum), the tissues were fixed in collidine-buffered 1% osmium tetroxide (1 volume of 0.2M s-collidine and 2 volumes of 2% osmium tetroxide, Electron Microscopy Sciences, Hatfield, PA) for 1 h and then rapidly dehydrated through 50, 80, 95% and absolute alcohols containing 2% lanthanum. Following dehydration, tissues were embedded in Epon 812-Araldite 506 Electron Microscopy Sciences, Hatfield, PA). Thin sections were prepared for light microscopy using routine procedure. Selected ultra-thin sections (90 nm) were mounted on 100-mesh copper grids and lightly contrasted with 2% uranyl acetate in distilled water for 1 h and 0.5% lead citrate in distilled water for 30 min. The grids were examined in a JEOL 1230 JEM transmission electron microscope (JEOL USA, Peabody, MA) using an AMT ORCA HR High Resolution camera with 2400 x 2400 pixel format.

SDS-PAGE electrophoresis and immunoblotting

Whole testes were flash-frozen in liquid nitrogen, and then ground to a fine powder. The tissue powder was then suspended in NaHCO3 buffer (1mM NaHCO3 and 1mM PMSF, pH 7.5) at a concentration of 100 mg tissue per 1ml buffer. The tissues were sonicated for 16 seconds at 30W power, and then cooled on ice for 30 minutes. The samples were then boiled in 1x Laemmli buffer at a final concentration of 25mg tissue per 1ml buffer. The samples were resolved on a 10% SDS-PAGE gel, and transferred to a PVDF membrane (Immunobilon-P; Millipore,

Billerica, MA). The blots were rinsed in PBS-T (PBS and 0.1% Tween-20), and then blocked in PBS-T with 5% w/v non-fat dry milk for 30 minutes at 37°C. The blots were then incubated with primary antibodies.

The blots were then washed three times in PBS-T, and incubated with goat anti-rabbit HRP secondary antibody (Bio-Rad, Hercules, CA) at 37°C for 30 minutes. The blots were again washed three times in PBS-T and developed with the ECL Plus detection reagent (GE Healthcare, Buckinghamshire, UK).

Quantitative PCR analysis of Tight Junction components

To analyze any changes in the expression of tight junction components, whole testes were flash-frozen in liquid nitrogen and ground to a fine powder using a mortar and pestel. The powdered tissue was then homogenized using a QIAShredder™ column and total RNA was extracted using the RNeasy Mini Kit (Qiagen, Germantown, MD). The RNA was then reverse transcribed using SuperScript® First-Strand synthesis system (Invitrogen, Camarillo, CA). Quantitative PCR was then performed on the cDNA (see supplemental table 2) using SYBR® Green Master Mix (Applied Biosystems, Foster City, CA), and analyzed on an ABI 7500 Real Time PCR Machine (Applied Biosystems, Carlsbad, California). The specificity of each PCR product was verified by sequencing the qPCR product. To verify primer products not amplified within the testis, a cDNA pool derived from mouse testis, kidney, liver, intestine, lung and thymus was used. Statistical analysis was performed using an unpaired two-tail student's t-test.

FIGURE 1.

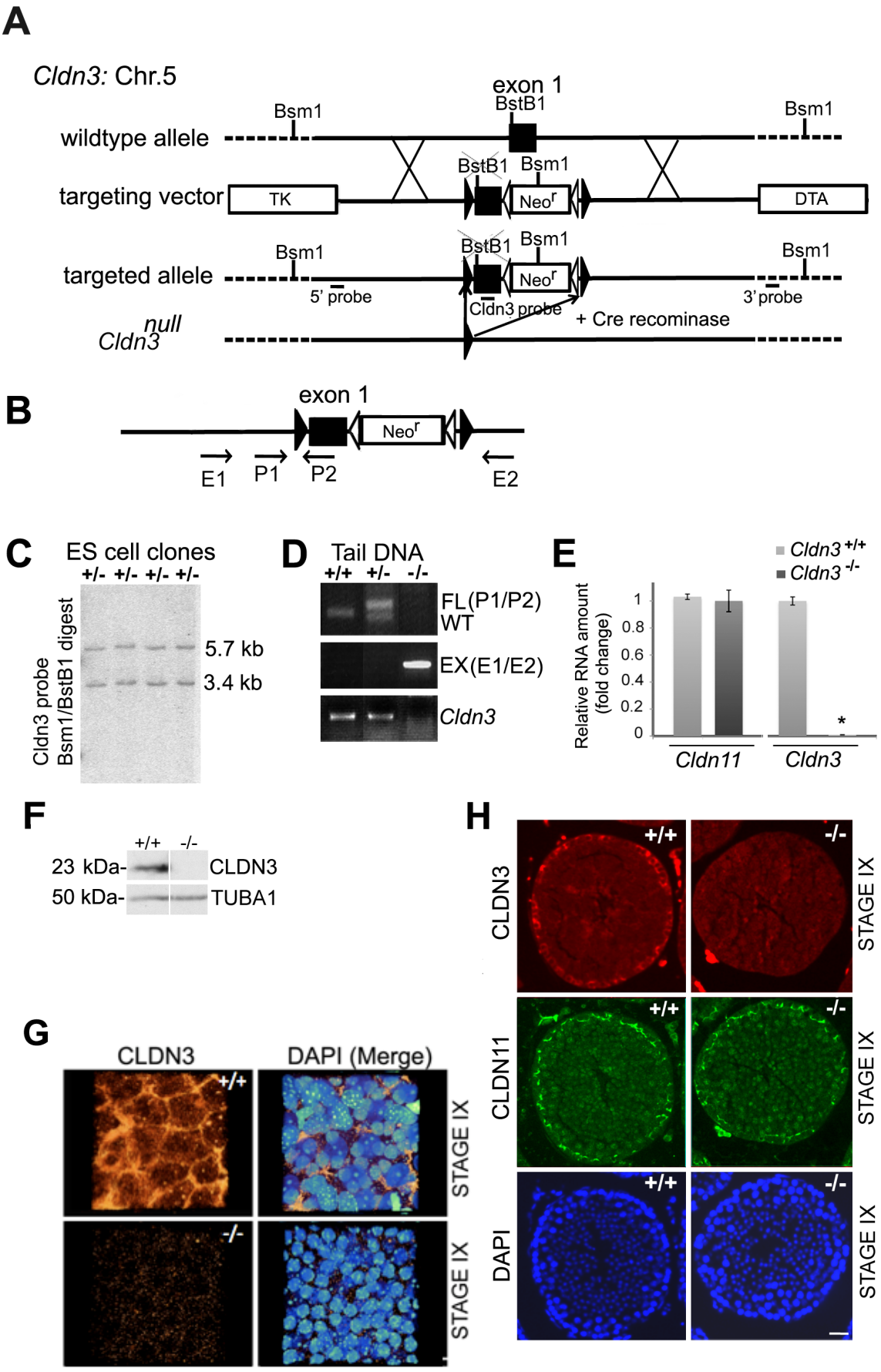
A
Cldn3: Chr.5
exon 1
BstB1
Bsm1
wildtype allele
targeting vector
TK
Neo^r
DTA
targeted allele
5' probe
3' probe
Cldn3 probe
+ Cre recominase
null Cldn3
B
exon 1
Neo^r
E1
P1
P2
E2
C
ES cell clones
+/- +/- +/- +/-
Cldn3 probe
Bsm1/BstB1 digest
5.7 kb
3.4 kb
D
Tail DNA
+/+ +/- -/-
FL(P1/P2) WT
EX(E1/E2)
Cldn3
E
Cldn3 +/+
Cldn3 -/-
Relative RNA amount (fold change)
1
0.8
0.6
0.4
0.2
0
*
Cldn11
Cldn3
F
+/+ -/-
23 kDa-
CLDN3
50 kDa-
TUBA1
G
CLDN3
DAPI (Merge)
+/+
-/-
STAGE IX
H
CLDN3
CLDN11
DAPI
+/+
-/-
STAGE IX

FIGURE 1. **Creation and validation of a conditional *Cldn3* KO allele. (A)** Schematic representation of the mouse *Cldn3* locus, *Cldn3* gene targeting vector used to generate a targeted *Cldn3* allele in ES cells, primary gene targeting product (conditional *Cldn3* null allele) and null allele produced from Cre recombinase mediated excision of the *Cldn3* exon and the neomycin resistance (Neo^r) gene cassette. TK, herpes simplex virus thymidine kinase gene; DTA, Diphtheria Toxin Alpha chain gene; open triangle, FRT site; black triangle, loxP site. The location of the Southern blot probes (5p, 3p and *Cldn3* ORF probe, black bars) and the restriction sites used are indicated. **(B)** Small arrowheads indicate relative positions of forward and reverse PCR primers used to confirm gene targeting (P1 and P2) or Cre-mediated recombination product (E1 and E2), or for genotyping. **(C)** Genomic DNA obtained from tail samples were screened for correct targeting of *Cldn3* by Southern blotting. The blot shows several correctly targeted clones using the indicated restriction enzyme and probe. **(D)** PCR of tail DNA using forward and reverse primers shown in (B). PCR products of 127 and 161 bp are generated from *Cldn3* floxed and wild-type alleles, respectively. A PCR product of 315 bp confirms the deletion of the *Cldn3* (exon1)-Neo cassette in homozygous null *Cldn3* mice. **(E)** qRT-PCR analysis of *Cldn3* and *Cldn11* transcripts from adult testis of $Cldn3^{-/-}$ mice and litter mate controls showing a loss of *Cldn3* transcript (n=2, * indicates $P \leq 0.01$). **(F)** Western blot analysis of total testis protein extracts prepared from wild-type and *Cldn3* knockout mice probed with anti-CLDN3 antibody. α-Tubulin antibody was used as a loading control. **(G)** A 3-D confocal reconstruction of a stage IX whole mount seminiferous tubule immunostained for CLDN3 (red heatmap) and

counter stained with DAPI (blue heatmap, DNA). Absence of CLDN3 staining is observed in *Cldn3*$^{-/-}$ seminiferous tubules. Scale bar = 10 μm. **(H)** Immunofluorescence detection of CLDN3 (red) and CLDN11 (green) protein on adult testis cross-sections from control and *Cldn3*$^{-/-}$ mice. CLDN3 protein was absent in *Cldn3*$^{-/-}$ stage IX tight junctions marked by CLDN11. Staging was confirmed by the counterstain DAPI (blue). Scale bar = 10 μm.

FIGURE 2.

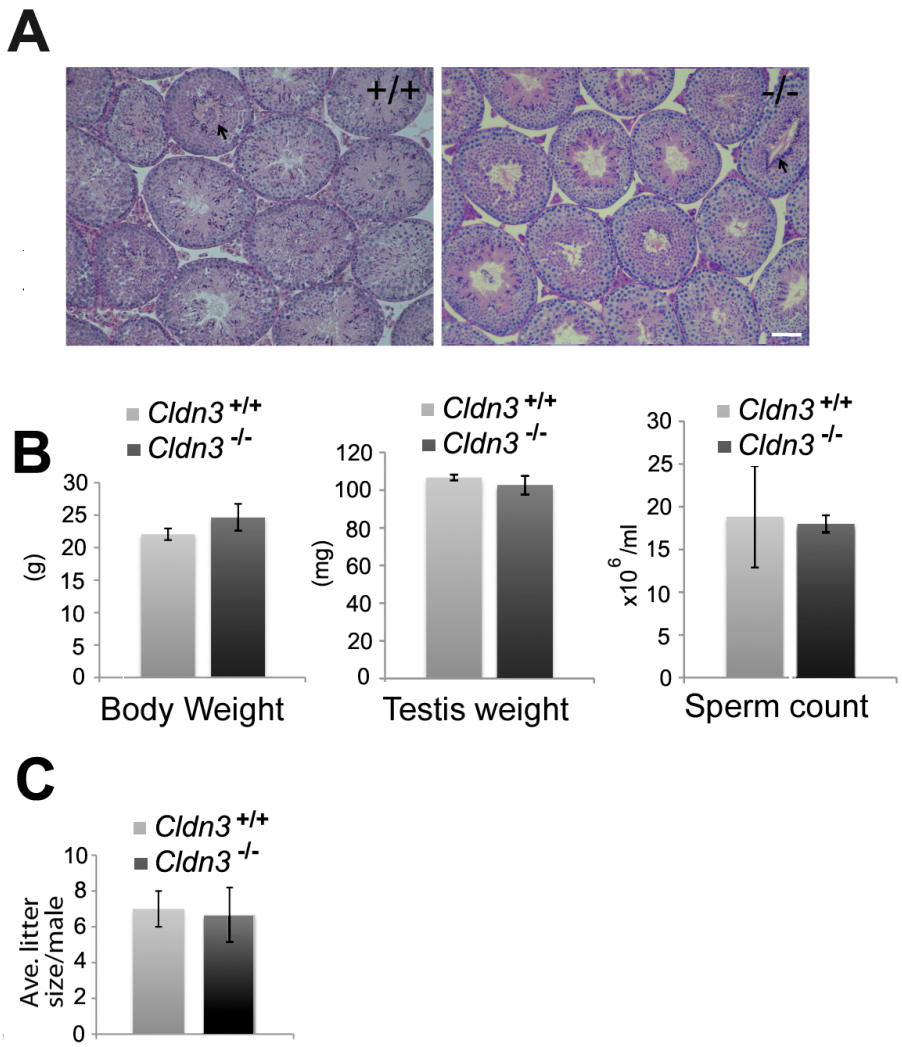

FIGURE 2. **CLDN3, a component of the SCTJ, is not necessary for spermatogenesis. (A)** Periodic acid Schiff's (PAS) stained testis cross-sections of control and *Cldn3*$^{-/-}$ mice at 10 weeks. Knockout testis sections confirm the presence of all cell types and normal spermiation (arrow) in stage VIII tubules. **(B)** Body weight and testis weight were measured in control and knockout males at 10 weeks (n=5). In comparison to control mice, knockout males showed no change in body weight; testis weight and epididymal sperm count. **(C)** Fertility testing showed that adult *Cldn3* knockout males were fertile relative to age matched control males, when mated to 12-week old fertile FVB/NJ females. (Error bars represent SEM).

FIGURE 3.

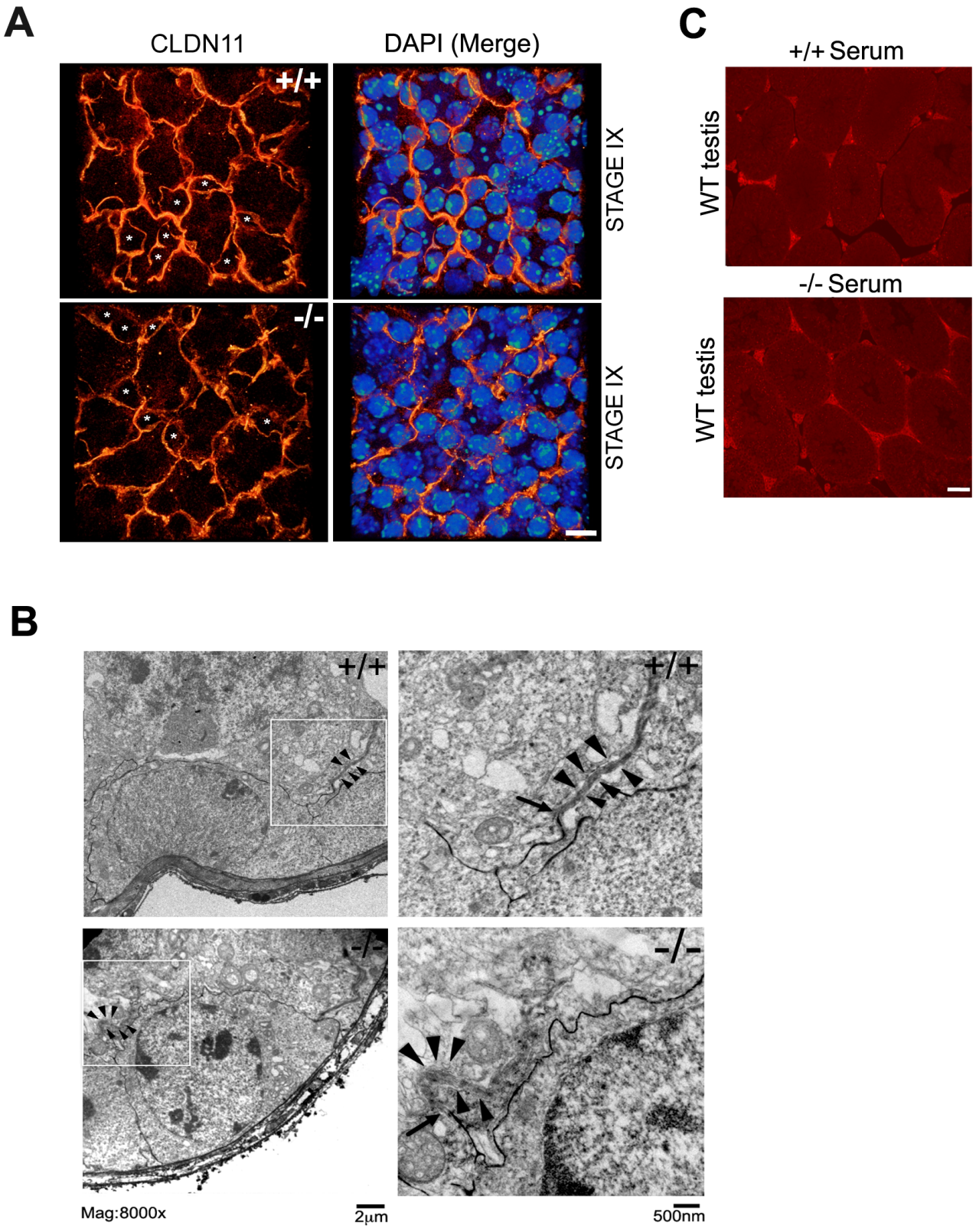
A
CLDN11
DAPI (Merge)
+/+
-/-
STAGE IX
STAGE IX
C
+/+ Serum
WT testis
-/- Serum
WT testis
B
+/+
+/+
-/-
-/-
Mag:8000x
2μm
500nm

FIGURE 3. **SCTJ barrier integrity is maintained in the absence of CLDN3. (A)** A 3-D confocal reconstruction of a stage IX whole-mount seminiferous tubule immunostained with CLDN11 (red heatmap) to mark SCTJs. Nuclei were counter stained with DAPI (blue, heatmap). Migrating preleptotene spermatocytes were observed enclosed within the SCTJs in stage IX of the seminiferous epithelium cycle in both control and *Cldn3*$^{-/-}$ mice. Scale bar = 10 μm. **(B)** Electron micrographs of lanthanum colloid tracer studies. EM analysis of testis perfused with lanthanum nitrate (tracer) was performed. The lanthanum tracer (black) permeates across the incomplete system of TJs of the myoid cell layer into the intercellular space between Sertoli cells and spermatogonia (I and III), where it is blocked by the SCTJs. Inset (II and IV) shows highlighted regions of both control and mutant sections. SCTJs are indicated with black arrowheads. Diffusion of the tracer into the adluminal compartment was occluded both by the control and *Cldn3*$^{-/-}$ SCTJ barrier. Black arrows mark the point at which the diffusion of the tracer is restricted by the SCTJs. **(C)** Immunofluorescence detection of testicular autoantibodies in control and *Cldn3* knockout sera. Testis sections from 129/SvJ mice were stained with serum sample from control and *Cldn3* knockout male mice. No testicular autoimmunity was detected in either serum sample. Data shows a representative image of one out of the six samples (n=6) analyzed. Scale Bar = 20 μm.

FIGURE 4.

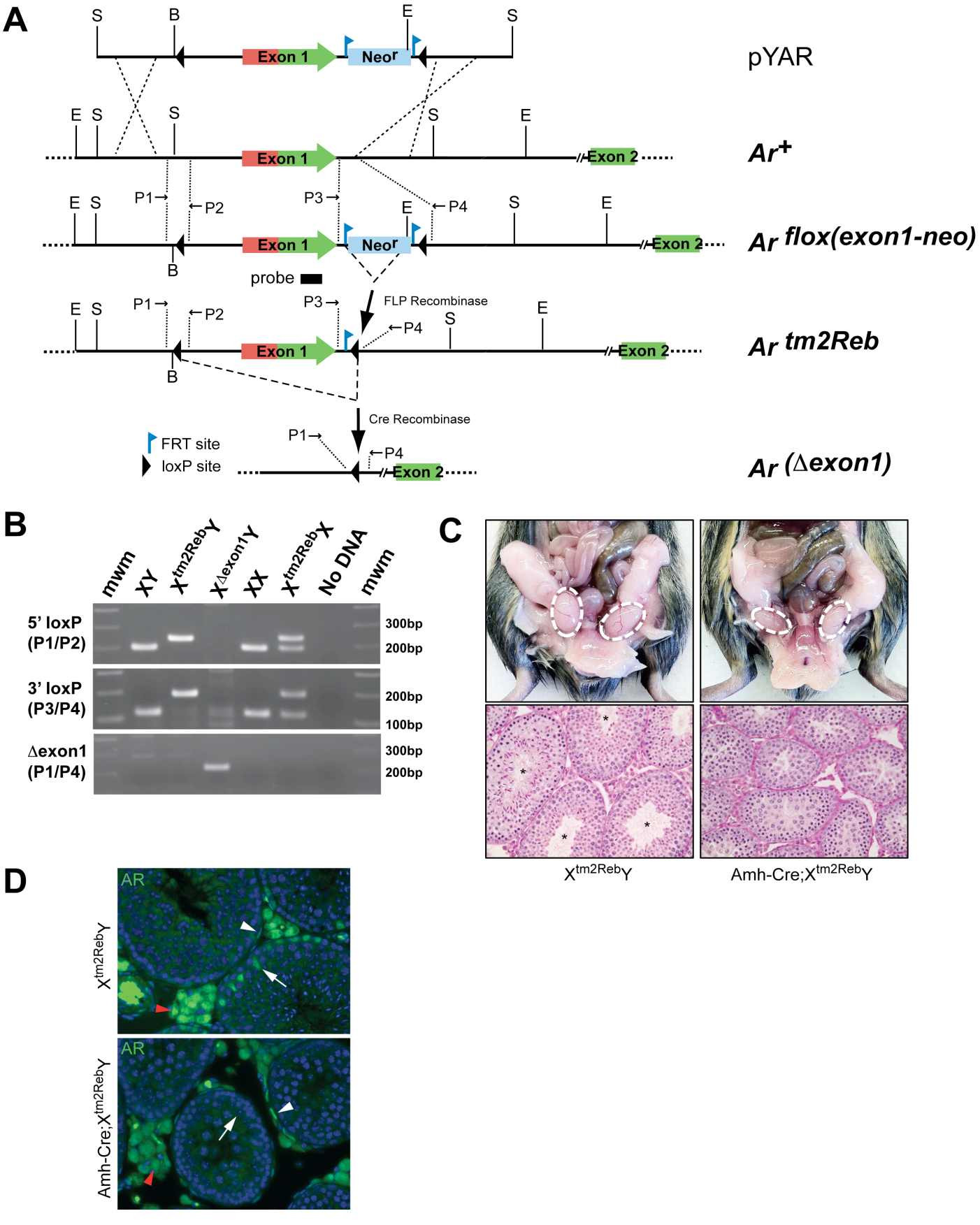
A
S
B
E
S
Exon 1
Neor
pYAR
E S
S
S
E
Exon 2
Ar+
P1
P2
P3
P4
B
probe
Ar flox(exon1-neo)
FLP Recombinase
Ar tm2Reb
Cre Recombinase
FRT site
loxP site
Ar (Δexon1)
B
mwm
XY
X tm2Reb Y
X Δexon1 Y
XX
X tm2Reb X
No DNA
mwm
5' loxP
(P1/P2)
3' loxP
(P3/P4)
Δexon1
(P1/P4)
300bp
200bp
200bp
100bp
300bp
200bp
C
X tm2Reb Y
Amh-Cre;X tm2Reb Y
D
AR
X tm2Reb Y
AR
Amh-Cre;X tm2Reb Y

FIGURE 4. **Generation of conditional exon 1 androgen receptor allele. (A)** Schematic representation of the 5' region of the mouse *Ar* locus (Ar^{+}), *Ar* gene targeting vector (pYAR), primary gene targeting product ($Ar^{flox(exon1\text{-}neo)}$), FLP recombinase mediated removal of the neomycin (Neo^{r}) gene cassette to produce a "silent" conditional allele (Ar^{tm2Reb}) and the deleted exon 1 allele post-Cre mediated recombination ($Ar^{(Dexon1)}$). Green and red portions of exons represent coding and 5' UTR sequence respectively. **(B)** PCR genotyping assay of loxP sites and deleted exon 1 allele (post-Cre recombination) using different primer combinations (see map). **(C)** Testes and PAS stained histological testis sections from control ($X^{tm2Reb}Y$) and Sertoli cell specific *Ar* deletion (Amh-Cre;$X^{tm2Reb}Y$) mice. Control mice show tubules with elongating/elongated spermatids (*) while mutants show a complete absence. **(D)** N-terminal directed AR antibody staining (green) in testes from control and Amh-Cre;$X^{tm2Reb}Y$ mice. AR Sertoli cell expression (white arrow) is absent in the mutant while Leydig (red arrowhead) and peritubular myoid cells (white arrowhead) continue to express AR.

FIGURE 5.

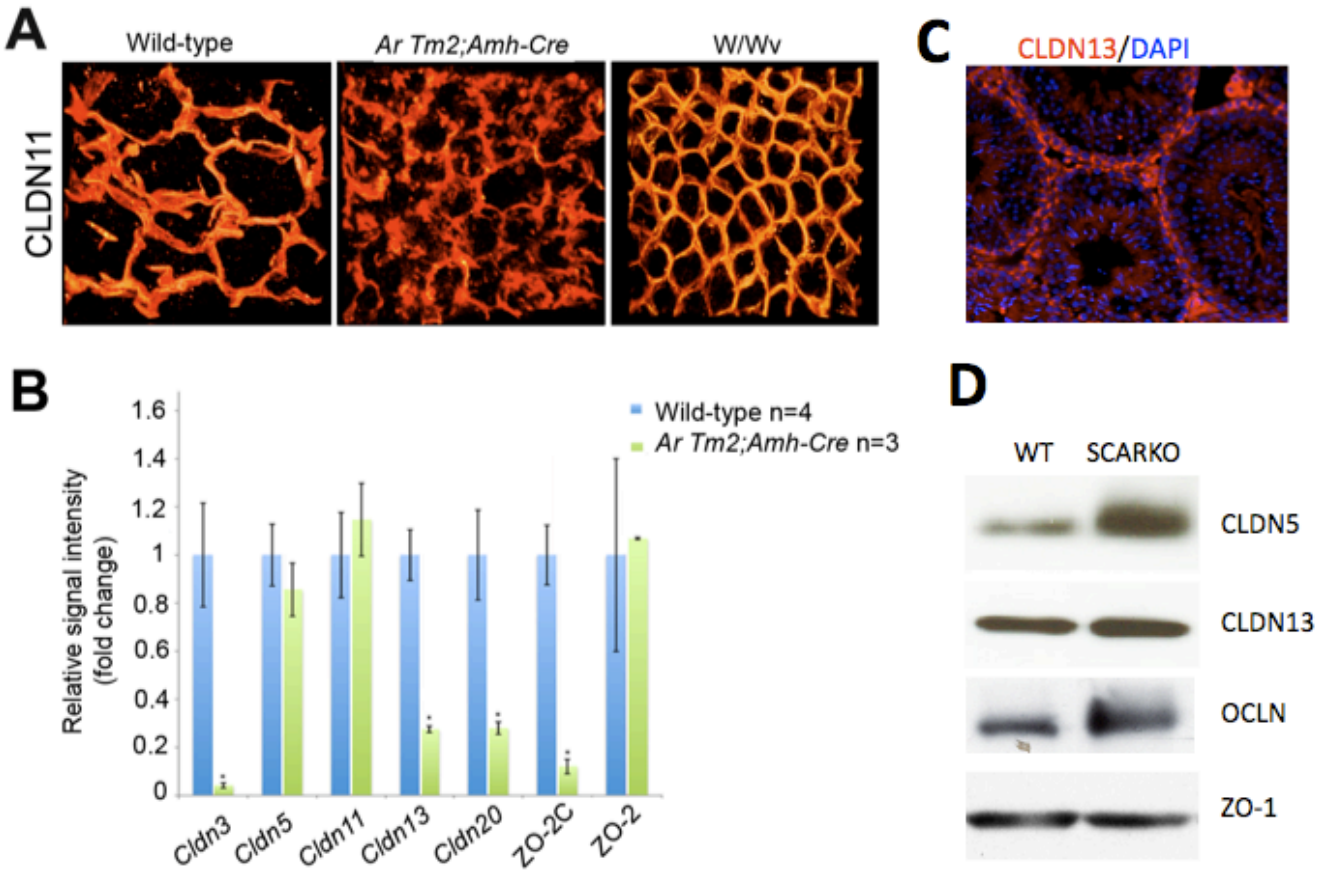

FIGURE 5. **SCTJ composition is compromised in SCARKO testis. (A)** A 3-D confocal reconstruction of whole-mount seminiferous tubules from wild-type, Amh-Cre;$X^{tm2Reb}Y$ and W/W^{v} mice immunostained with CLDN11 (red heatmap). Amh-Cre;$X^{tm2Reb}Y$ mutant animals have severely disorganized SCTJs. W/W^{V} mice testes, which are nearly devoid of all germ cells have proper CLDN11 localization and SCTJ organization. **(B)** qRT-PCR analysis on total RNA from testis of adult wild-type and Amh-Cre;$X^{tm2Reb}Y$ mutant mice show a substantial downregulation of *Cldn3, Cldn13, Cldn20, ZO-2C* mRNA expression. (* indicates $P \leq 0.01$). **(C))** Immunofluorescence detection of CLDN13 (red) and DNA (DAPI; blue) on adult testis cross-sections from wild-type mice. Typical basal SCTJ-type staining pattern was observed for CLDN13. **(D)** Western blot analysis of total testis protein extracts

prepared from wild-type and SCARKO mice probed with anti-CLDN5, anti-CLDN13, anti-OCLN and anti-ZO-2 antibody. There was a greater enrichment for CLDN5 and OCLN in the SCARKO testis, while CLDN13 and ZO-2 were found to be in equal abundance in the wild-type and SCARKO testes.

FIGURE 6.

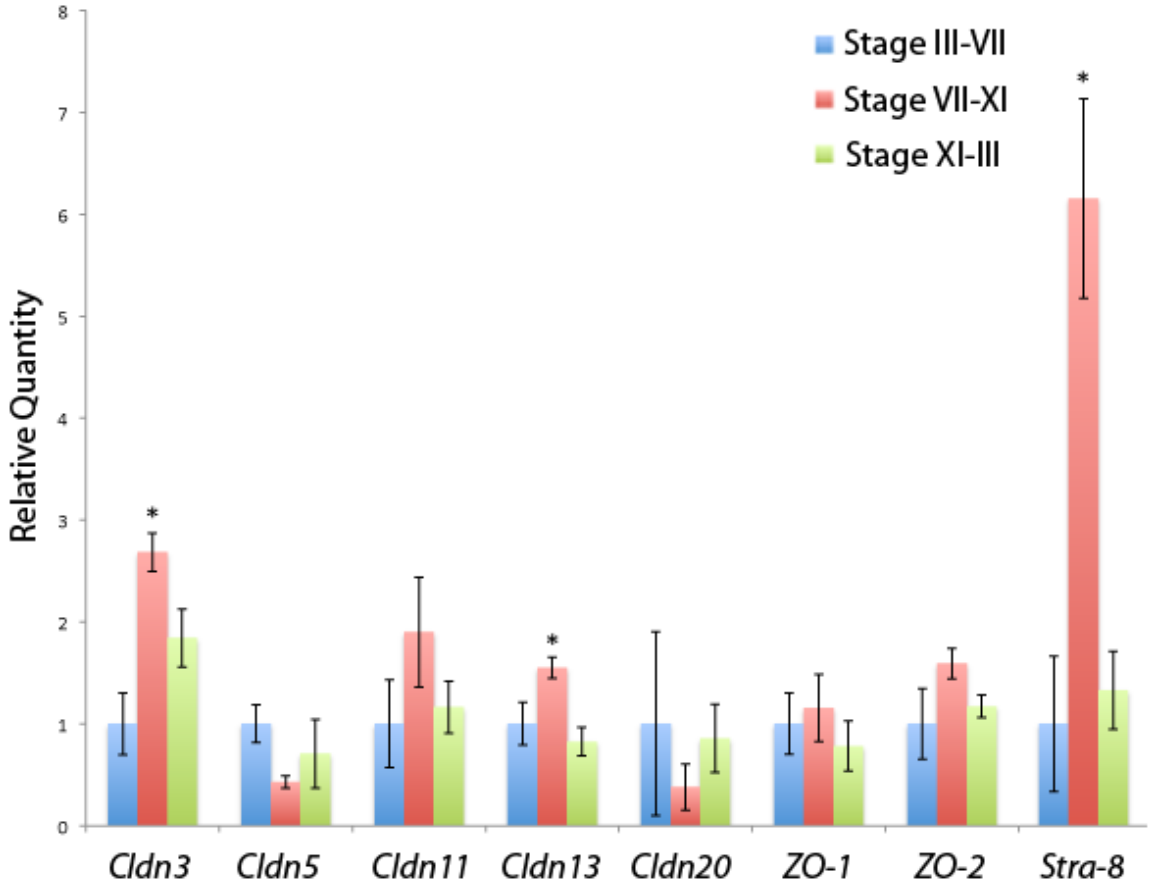

FIGURE 6. **Peak expression of both *Cldn13* and *Cldn3* mRNA is observed in stages VII- XI; stages of highest androgen receptor expression. (A)** qRT- PCR analysis of tight junction components performed on total RNA obtained from transillumination dissection of seminiferous tubules at different stages of the seminiferous cycle. *Stra8* is used as a marker of stages VII- XI. (* indicates $P \leq 0.05$).

FIGURE S1.

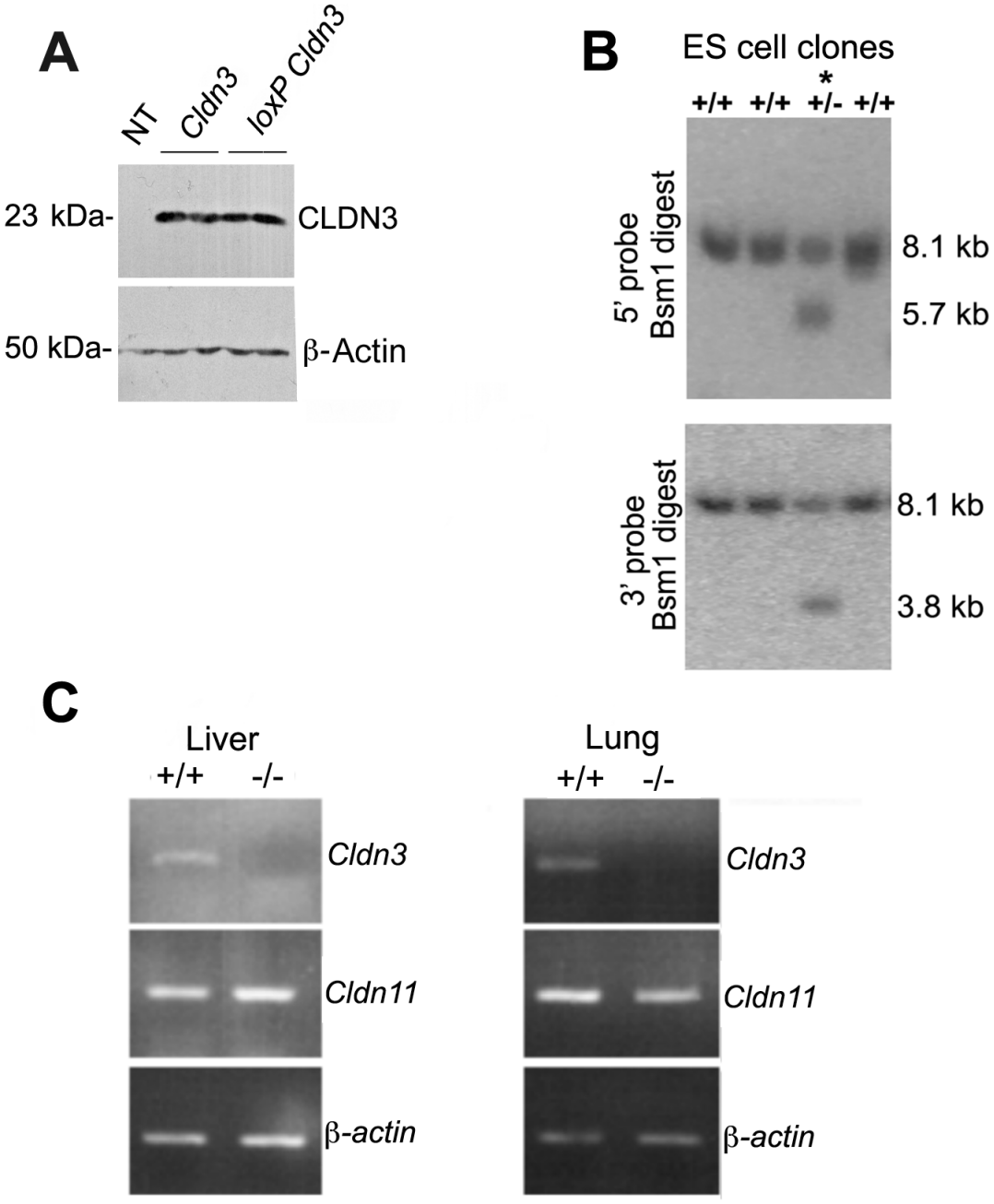
A
NT
Cldn3
loxP Cldn3
23 kDa-
CLDN3
50 kDa-
β-Actin
B
ES cell clones
*
+/+ +/+ +/- +/+
5' probe
Bsm1 digest
8.1 kb
5.7 kb
3' probe
Bsm1 digest
8.1 kb
3.8 kb
C
Liver
+/+ -/-
Cldn3
Cldn11
β-actin
Lung
+/+ -/-
Cldn3
Cldn11
β-actin

SUPPLEMENTARY FIGURE S1. **Validation experiments for generation of Cldn3 conditional knockout mouse.** (A) Western blot analysis on HeLa cells transfected with pCMV-Cldn3 or pCMV-loxP-Cldn3 (loxP sequence was cloned into the 5pUTR region of the *Cldn3* gene). Insertion of the loxP sequence in the 5pUTR of the gene did not alter its protein expression. (B) Neomycin-resistant ES cell clones were screened for correct targeting of *Cldn3* by Southern blotting of genomic DNA. The blot shows one correctly targeted clone using the indicated restriction enzyme and probe. (C) RT-PCR on total RNA obtained from lung and liver tissues of wild-type and *Cldn3*$^{-/-}$ mice confirmed the absence of *Cldn3* transcript in these tissues.

FIGURE S2.

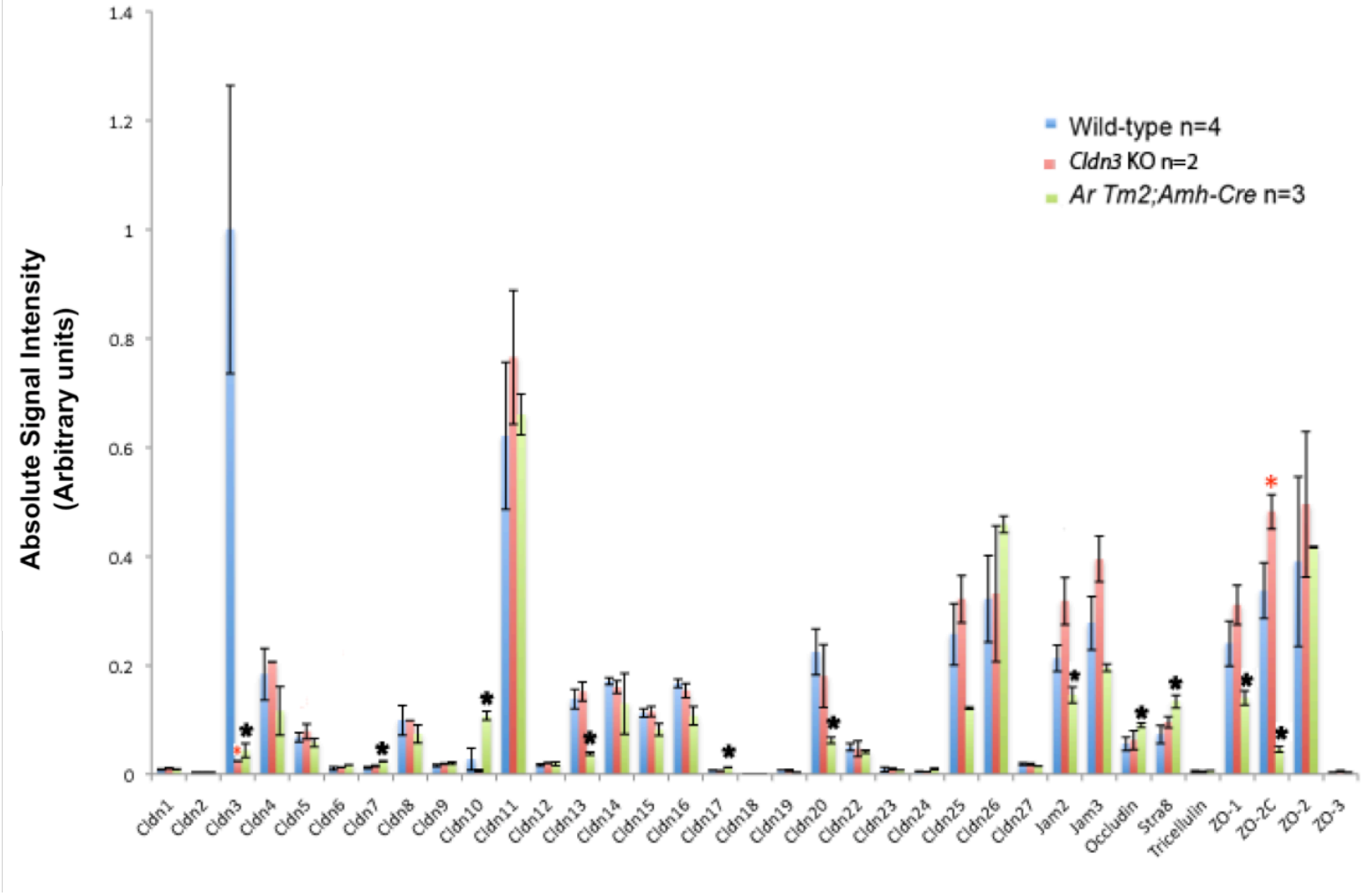

SUPPLEMENTARY FIGURE S2. **Relative expression of tight junction components in the *Cldn3* knockout and SCARKO mouse.** Whole testis RNA was extracted from wild-type (n=3), *Cldn3* knockout (n=2), and SCARKO mice (n=2). Real-time PCR was performed on cDNA, and was normalized to total RNA loading. Each primer set was verified by sequencing of the resulting PCR product. Any differential gene expression that was found to be significant (student's t-test, $p<0.05$) is marked with an asterisk. Only *Cldn3* and *ZO-2C,* marked with a red asterisk were significantly different in the *Cldn3* knockout mouse when compared to the wild-type. All genes marked with a black asterisk were significantly different in the SCARKO animals compared to wild-type.

SUPPLEMENTARY TABLE 1. Oligonucleotide primers used for Southern blot probes.

Probe	Forward Primer (5' -> 3')	Reverse Primer (5' -> 3')
Cldn3 ORF probe	CCCACCGCGCGACAAGTATGC	TCATGGTTTGCCTGTCTCTG
Cldn3 3' probe	AACCCGGGAGTTGTTAACACA GAGATGGCAGC	GGCATTCCTTAAGAAGAGGAGA AACATTAAGC
Cldn3 5' probe	CAACACACCTGGCTAGACGT	GACTCTCTTGTCCCCCACC

SUPPLEMENTARY TABLE 2. Oligonucleotide primers used for real-time PCR

Gene	Forward Primer (5' -> 3')	Reverse Primer (5' -> 3')
Actb	GGCTGTATTCCCCTCCATCG	CCAGTTGGTAACAATGCCATGT
Cldn1	GGATGGCTGTCATTGGGGGCA	GCAGCGGCCCAGCCAGTAAA
Cldn2	GGCTGTTAGGCACATCCAT	TGGCACCAACATAGGAACTC
Cldn3	GTCGTTCCCGGCGACAGACG	AACGCGCCACATGGGAAGGG
Cldn4	GCTGGCTTTGTGTCCCTGAGGC	GCCGATGAAGGCGGTCACCC
Cldn5	AGGCACCAAACTGCCGCGAA	CCCCACCTTGGGGGAGTGCT
Cldn6	CAGGGGTGGCCGAACCGGA	CCACGACGATGCTGTTGCCG
Cldn7	AGGGTCTGCTCTGGTCCTT	GTACGCAGCTTTGCTTTCA
Cldn8	GTGCTGCGTCCGTCTTGGCT	GCTCGCGCTTTAGGGCCACA
Cldn9	AGTGGCACCTCACGGTTCCC	GCTGCGGGCCTCTCACACATC
Cldn10	CCCAGAATGGGCTACACATA	CCTTCTCCGCCTTGATACTT
Cldn11	GGCCAAGTACAGGCGAGCCC	TCCCCGGAGCAGCAGACGAT
Cldn12	CGGCTTCGCCAGAACGCACTT	AGCAGCCTGTCTGCGCCTCT
Cldn13	TCCCCGTTGCATTGAGACCCCT	AGCTAGCCGCATCCAGAGTCCA
Cldn14	TGTAGGGCGCACTGGCTGGTT	TGGTCCTTAGGTGCCCGCAG
Cldn15	TCCGTCCATGCTGGCCCTCT	CCACGTTGGTGCAGCGGAGT
Cldn16	CCGCCTTTGCTTTGTTGCAGGG	ACCCAGCCATTCCAAGCCAGC
Cldn17	TCGTTCTGATTCCAGTGTCC	TCCTCCAAGTTCTCGCTTCT
Cldn18	GACCGTTCAGACCAGGTACA	GCGATGCACATCATCACTC
Cldn19	CCCAGCACTCCTGTCAATGCC	TACTCTCTGGCAGCAGTTGAGGG
Cldn20	TCGGCAGGTCTCCAGCTCCTT	GCAGTCCACCCACAACCCCTG
Cldn22	CTTCCGAACGGCAACGCAGG	TGCCTCCCGACTTCCTCCTGG
Cldn23	TGGAGTCTGAGGGTGACTTGAACTTCTG	AAGGAAGGCTTGACCTCCAGTTAGAGGAAG
Cldn24	GATCATGGTTCATACCTAG	TAAGGACACGACTCGGC
Cldn25	ACGAGCAGTTCATGGAGAAG	CAAAGCACATCAAGCCCAAG
Cldn26	ATGAACCCTTTCTGGCAGG	AACACCATCACGATCAGACTG
Cldn27	ATCGTATGTGGTTGGGTCTG	GGTGTGAGTAGCTGATGTAGATG
Jam2	GAGTGGAAGAAGGTGGGACA	AGGAACAGCAGGAGCCACTA
Jam3	GAACTCGGAGACAGGCACTC	CGTCTGTACGCACAGCAGAT
Occludin	GAGTTAACGTCGTGGACCGGTATC	CCCTGAAATACAAAGGCAGGAATG
Stra8	AGTCTGATATCACAGCCTCAAAG	CATTCTCGGAATACATTCTGGCA
Tricellulin	AAGACCCCCTTCGTACTCGT	GAACATCGCATTCATTGGTG
ZO-1	CCACCCCCATCTCAGAGTAA	CACCGGAGTGATGGTTTTCT
ZO-2	AGCCAGATGCTGGCCTCCCCC	ACCACGCTTCGAGTGTGCTGC
ZO-2C	GCTTCCAGAAATGGGTGAAA	TGCTCCCATATCACCTCCTC
ZO-3	GTGTCGTGAGCTTCCCCAAG	ATGGCATACCATTCACCTGCA

DISCUSSION AND FUTURE DIRECTIONS

The fact that the Sertoli cell tight junction (SCTJ) barrier remains intact in mice lacking claudin-3 (CLDN3) and yet the barrier is compromised in multiple Sertoli cell androgen receptor knockout (SCARKO) models suggests that AR mediated CLDN3 expression is not essential for the remodeling and maintenance of the SCTJ barrier. However, the additional observation that the transient localization of CLDN3 to the SCTJs is conserved between mice and humans presents a compelling yet paradoxical argument that CLDN3 must be playing an essential role within the testis for its expression to remain conserved over approximately 100 million years of evolutionary divergence between rodents and humans (Nei et al., 2001).

One explanation of how a gene such as CLDN3 would have such highly conserved expression and yet the *Cldn3* knockout mouse having no associated phenotype would be that the gene is protecting against a stressor that the laboratory mouse is no longer exposed to, and therefore the expression of CLDN3 is merely vestigial. One such stressor would be an immunity related phenotype. Not only are laboratory mice housed in pathogen-free environments, but it is also known that common strains of laboratory mice have reduced autoimmune phenotypes relative to humans (Kekalainen et al., 2007; Mathis and Benoist, 2007; Morel, 2004), and that knockout lines often need to be back-crossed to mouse strains susceptible to autoimmunity in order for autoimmune phenotypes to present themselves.

It is equally probable, however, that there may be a compensatory mechanism at play mitigating the effects of the lack of CLDN3. Whether the lack of phenotype can be explained via the lack of an appropriate stimulus or due to genetic robustness, as can often be the case with knockout mice (Barbaric et al., 2007), it may be more prudent to take an unbiased approach in characterizing the knockout mice, rather than iteratively trying various challenges or combinatorial knockouts of other claudins, in the hopes of generating a more striking phenotype.

One such unbiased approach would be to perform microarray analysis comparing wild-type and *Cldn3*$^{-/-}$ tissues that normally express CLDN3 in the adult, including the brain, lung, thymus, liver, kidney, intestine, and testis (Hamazaki et al., 2007; Holmes et al., 2006; Liebner et al., 2008; Meng et al., 2005; Morita et al., 1999a). Ideally, one could tease out a common compensatory mechanism between most if not all tissues, by looking for genes and/or genetic pathways that are differentially expressed across multiple CLDN3 expressing tissues. Conversely, it is possible that CLDN3 plays a unique role in each of these tissues, and that each tissue would therefore have its own compensatory mechanism. Thirdly, there could be no differential expression of genes between the wild-type and knockout tissues. This would suggest that CLDN3 is protecting the mice against a stressor that they would encounter in their native environment, such as a pathogen, and that since these stressors are no longer present in their native environment, the continued expression of CLDN3 in laboratory strains is merely a vestigial trait. And finally, there could be a molecular phenotype associated with a loss of CLDN3 that does not present itself as an obvious overt phenotype. These could include mild

inflammatory responses, or ectopic activation of various genetic pathways that are not overtly detrimental.

Any of the positive outcomes proposed could be verified by further experimentation. If a compensatory pathway is identified, then the compensation can be pharmacologically or genetically removed. Compensation would be confirmed if the combination of a lack of the compensatory pathway and CLDN3 resulted in a more severe phenotype than either of the two knockouts by themselves. If there is a molecular phenotype, this can be verified by challenging the mice with compounds that would aggravate the molecular phenotype. The hypothesis would be that the lack of CLDN3 has sensitized the mice to a particular pathogenesis. For example, if an increase in the expression of cytokines was detected in the intestine, the mice would therefore be sensitized to developing inflammatory bowel disease, and thus this sensitivity could be unmasked by then treating the mice with dextran sodium sulfate (Xavier and Podolsky, 2007).

However, if there is not a phenotypic difference between the *Cldn3*-knockout mice and wild-type mice, then this result would be very useful for current clinical trials targeting CLDN3. Upregulation of claudin-3 transcript and protein is already used in the clinic as a diagnostic marker for bone, brain and ovarian cancers (Morin, 2005; Sukumar and Kominsky, 2012). In addition to being used as a marker, CLDN3 and CLDN4 are being targeted as potential therapeutic targets using *Clostridium perfringens* enterotoxin (CPE) which binds to CLDN3 and CLDN4 and then forms pores which kills the host cell (Gao and McClane, 2012). More recently, researchers have also been using the C-terminal fragment of CPE (C-CPE), which

contains the claudin binding domain, but lacks the pore forming domain which may have toxic effects on other CLDN3 and CLDN4 expression tissues within the patient (Gao and McClane, 2012). The hypothesis is that by disrupting the CLDN3 and CLDN4 tight junctions of the tumor, the tumor will become more vulnerable to chemotherapy treatment. This hypothesis can be directly tested using the *Cldn3* knockout mouse, by crossing the knockout allele onto mouse models of CLDN3 expressing cancers, and determine whether the disruption of CLDN3 tight junctions in these tumors is sufficient to explain the mode of action of C-CPE.

One such mouse is the *p63* knockout mouse, which is used as a model for Barrett's esophagus, and has a 43-fold increase in *Cldn3* expression in the stomach metaplasias that form in this mouse compared to normal stomach tissue, which correlates with an upregulation of CLDN3 observed in similar metaplasias from human patients (Wang et al., 2011). Therefore, it would be very interesting to compare CPE and C-CPE treatment in these mice with a *Trp63*$^{-/-}$*; Cldn3*$^{-/-}$ double knockout. This would help to determine whether the hypothesis, that C-CPE therapy works by disrupting CLDN3 tight junctions and therefore allowing chemotherapy drugs to penetrate further into tumors, is correct. Determining the exact mode of activity for C-CPE is essential to understanding how C-CPE treatment effects tumor biology, and therefore which chemotherapy treatments would be best suited to be used in conjunction with C-CPE.

BIBLIOGRAPHY

Barbaric, I., G. Miller, and T.N. Dear. 2007. Appearances can be deceiving: phenotypes of knockout mice. *Brief Funct Genomic Proteomic*. 6:91-103.

Bremner, W.J., M.R. Millar, R.M. Sharpe, and P.T. Saunders. 1994. Immunohistochemical localization of androgen receptors in the rat testis: evidence for stage-dependent expression and regulation by androgens. *Endocrinology*. 135:1227-34.

Cavicchia, J.C., and F.L. Sacerdote. 1988. Topography of the rat blood-testis barrier after intratubular administration of intercellular tracers. *Tissue and Cell*. 20:577-86.

Chang, C., Y.T. Chen, S.D. Yeh, Q. Xu, R.S. Wang, F. Guillou, H. Lardy, and S. Yeh. 2004. Infertility with defective spermatogenesis and hypotestosteronemia in male mice lacking the androgen receptor in Sertoli cells. *Proc Natl Acad Sci U S A*. 101:6876-81.

Chihara, M., S. Otsuka, O. Ichii, Y. Hashimoto, and Y. Kon. 2010. Molecular dynamics of the blood-testis barrier components during murine spermatogenesis. *Mol Reprod Dev*. 77:630-9.

Daugherty, B.L., C. Ward, T. Smith, J.D. Ritzenthaler, and M. Koval. 2007. Regulation of heterotypic claudin compatibility. *J Biol Chem*. 282:30005-13.

De Gendt, K., J.V. Swinnen, P.T. Saunders, L. Schoonjans, M. Dewerchin, A. Devos, K. Tan, N. Atanassova, F. Claessens, C. Lecureuil, W. Heyns, P. Carmeliet, F. Guillou, R.M. Sharpe, and G. Verhoeven. 2004. A Sertoli cell-selective knockout of the androgen receptor causes spermatogenic arrest in meiosis. *Proc Natl Acad Sci U S A*. 101:1327-32.

Dohle, G.R., M. Smit, and R.F. Weber. 2003. Androgens and male fertility. *World J Urol*. 21:341-5.

Dym, M., and J.C. Cavicchia. 1977. Further observations on the blood-testis barrier in monkeys. *Biol Reprod*. 17:390-403.

Dym, M., and D.W. Fawcett. 1970. The blood-testis barrier in the rat and the physiological compartmentation of the seminiferous epithelium. *Biol Reprod*. 3:308-26.

Eacker, S.M., J.E. Shima, C.M. Connolly, M. Sharma, R.W. Holdcraft, M.D. Griswold, and R.E. Braun. 2007. Transcriptional profiling of androgen receptor (AR) mutants suggests instructive and permissive roles of AR signaling in germ cell development. *Mol Endocrinol*. 21:895-907.

Escudero-Esparza, A., W.G. Jiang, and T.A. Martin. 2011. The Claudin family and its role in cancer and metastasis. *Front Biosci*. 16:1069-83.

Fawcett, D.W., L.V. Leak, and P.M. Heidger, Jr. 1970. Electron microscopic observations on the structural components of the blood-testis barrier. *Journal of reproduction and fertility. Supplement*. 10:105-22.

Furuse, M. 2010. Molecular basis of the core structure of tight junctions. *Cold Spring Harb Perspect Biol*. 2:a002907.

Furuse, M., K. Fujita, T. Hiiragi, K. Fujimoto, and S. Tsukita. 1998a. Claudin-1 and -2: novel integral membrane proteins localizing at tight junctions with no sequence similarity to occludin. *J Cell Biol*. 141:1539-50.

Furuse, M., H. Sasaki, K. Fujimoto, and S. Tsukita. 1998b. A single gene product, claudin-1 or -2, reconstitutes tight junction strands and recruits occludin in fibroblasts. *J Cell Biol*. 143:391-401.

Furuse, M., H. Sasaki, and S. Tsukita. 1999. Manner of interaction of heterogeneous claudin species within and between tight junction strands. *J Cell Biol*. 147:891-903.

Gao, Z., and B.A. McClane. 2012. Use of Clostridium perfringens Enterotoxin and the Enterotoxin Receptor-Binding Domain (C-CPE) for Cancer Treatment: Opportunities and Challenges. *J Toxicol*. 2012:981626.

Gow, A., C. Davies, C.M. Southwood, G. Frolenkov, M. Chrustowski, L. Ng, D. Yamauchi, D.C. Marcus, and B. Kachar. 2004. Deafness in Claudin 11-null mice reveals the critical contribution of basal cell tight junctions to stria vascularis function. *The Journal of neuroscience : the official journal of the Society for Neuroscience*. 24:7051-62.

Gow, A., C.M. Southwood, J.S. Li, M. Pariali, G.P. Riordan, S.E. Brodie, J. Danias, J.M. Bronstein, B. Kachar, and R.A. Lazzarini. 1999. CNS myelin and sertoli cell tight junction strands are absent in Osp/claudin-11 null mice. *Cell*. 99:649-59.

Greenbaum, M.P., W. Yan, M.H. Wu, Y.N. Lin, J.E. Agno, M. Sharma, R.E. Braun, A. Rajkovic, and M.M. Matzuk. 2006. TEX14 is essential for intercellular bridges and fertility in male mice. *Proc Natl Acad Sci U S A*. 103:4982-7.

Griswold, M.D. 1998. The central role of Sertoli cells in spermatogenesis. *Semin Cell Dev Biol*. 9:411-6.

Haddad, N., J. El Andalousi, H. Khairallah, M. Yu, A.K. Ryan, and I.R. Gupta. 2011. The tight junction protein claudin-3 shows conserved expression in the nephric duct and ureteric bud and promotes tubulogenesis in vitro. *American journal of physiology. Renal physiology*. 301:F1057-65.

Hamazaki, Y., H. Fujita, T. Kobayashi, Y. Choi, H.S. Scott, M. Matsumoto, and N. Minato. 2007. Medullary thymic epithelial cells expressing Aire represent a unique lineage derived from cells expressing claudin. *Nat Immunol*. 8:304-11.

Hashizume, A., T. Ueno, M. Furuse, S. Tsukita, Y. Nakanishi, and Y. Hieda. 2004. Expression patterns of claudin family of tight junction membrane proteins in developing mouse submandibular gland. *Developmental dynamics : an official publication of the American Association of Anatomists*. 231:425-31.

Holash, J.A., S.I. Harik, G. Perry, and P.A. Stewart. 1993. Barrier properties of testis microvessels. *Proc Natl Acad Sci U S A*. 90:11069-73.

Holdcraft, R.W., and R.E. Braun. 2004a. Androgen receptor function is required in Sertoli cells for the terminal differentiation of haploid spermatids. *Development*. 131:459-67.

Holdcraft, R.W., and R.E. Braun. 2004b. Hormonal regulation of spermatogenesis. *Int J Androl*. 27:335-42.

Holmes, J.L., C.M. Van Itallie, J.E. Rasmussen, and J.M. Anderson. 2006. Claudin profiling in the mouse during postnatal intestinal development and along the

gastrointestinal tract reveals complex expression patterns. *Gene Expr Patterns*. 6:581-8.

Huckins, C. 1978. Spermatogonial intercellular bridges in whole-mounted seminiferous tubules from normal and irradiated rodent testes. *Am J Anat*. 153:97-121.

Hutson, J.M. 1986. Testicular feminization: a model for testicular descent in mice and men. *Journal of pediatric surgery*. 21:195-8.

Kekalainen, E., A. Miettinen, and T.P. Arstila. 2007. Does the deficiency of Aire in mice really resemble human APECED? *Nat Rev Immunol*. 7:1.

Kiuchi-Saishin, Y., S. Gotoh, M. Furuse, A. Takasuga, Y. Tano, and S. Tsukita. 2002. Differential expression patterns of claudins, tight junction membrane proteins, in mouse nephron segments. *Journal of the American Society of Nephrology : JASN*. 13:875-86.

Kohler, K., and A. Zahraoui. 2005. Tight junction: a co-ordinator of cell signalling and membrane trafficking. *Biol Cell*. 97:659-65.

Komljenovic, D., R. Sandhoff, A. Teigler, H. Heid, W.W. Just, and K. Gorgas. 2009. Disruption of blood-testis barrier dynamics in ether-lipid-deficient mice. *Cell and tissue research*. 337:281-99.

Kotaja, N., S. Kimmins, S. Brancorsini, D. Hentsch, J.L. Vonesch, I. Davidson, M. Parvinen, and P. Sassone-Corsi. 2004. Preparation, isolation and characterization of stage-specific spermatogenic cells for cellular and molecular analysis. *Nature methods*. 1:249-54.

Lewandowsky, M. 1900. Zur Lehre von der Cerebrospinalflüssigkeit *Zeitschrift für Klinische Medicin*. 40:480-494.

Liebner, S., M. Corada, T. Bangsow, J. Babbage, A. Taddei, C.J. Czupalla, M. Reis, A. Felici, H. Wolburg, M. Fruttiger, M.M. Taketo, H. von Melchner, K.H. Plate, H. Gerhardt, and E. Dejana. 2008. Wnt/beta-catenin signaling controls development of the blood-brain barrier. *J Cell Biol*. 183:409-17.

Masuda, S., Y. Oda, H. Sasaki, J. Ikenouchi, T. Higashi, M. Akashi, E. Nishi, and M. Furuse. 2011. LSR defines cell corners for tricellular tight junction formation in epithelial cells. *J Cell Sci*. 124:548-55.

Mathis, D., and C. Benoist. 2007. A decade of AIRE. *Nat Rev Immunol*. 7:645-50.

Matter, K., S. Aijaz, A. Tsapara, and M.S. Balda. 2005. Mammalian tight junctions in the regulation of epithelial differentiation and proliferation. *Curr Opin Cell Biol*. 17:453-8.

Mazaud-Guittot, S., E. Meugnier, S. Pesenti, X. Wu, H. Vidal, A. Gow, and B. Le Magueresse-Battistoni. 2010. Claudin 11 deficiency in mice results in loss of the Sertoli cell epithelial phenotype in the testis. *Biology of reproduction*. 82:202-13.

Meng, J., A.R. Greenlee, C.J. Taub, and R.E. Braun. 2011. Sertoli cell-specific deletion of the androgen receptor compromises testicular immune privilege in mice. *Biol Reprod*. 85:254-60.

Meng, J., R.W. Holdcraft, J.E. Shima, M.D. Griswold, and R.E. Braun. 2005. Androgens regulate the permeability of the blood-testis barrier. *Proc Natl Acad Sci U S A*. 102:16696-700.

Mineta, K., Y. Yamamoto, Y. Yamazaki, H. Tanaka, Y. Tada, K. Saito, A. Tamura, M. Igarashi, T. Endo, K. Takeuchi, and S. Tsukita. Predicted expansion of the claudin multigene family. *FEBS Lett*. 585:606-12.

Mineta, K., Y. Yamamoto, Y. Yamazaki, H. Tanaka, Y. Tada, K. Saito, A. Tamura, M. Igarashi, T. Endo, K. Takeuchi, and S. Tsukita. 2011. Predicted expansion of the claudin multigene family. *FEBS Lett*. 585:606-12.

Mintz, B., and E.S. Russell. 1957. Gene-induced embryological modifications of primordial germ cells in the mouse. *The Journal of experimental zoology*. 134:207-37.

Morales, C.R., and N.B. Hecht. 1994. Poly(A)+ ribonucleic acids are enriched in spermatocyte nuclei but not in chromatoid bodies in the rat testis. *Biology of reproduction*. 50:309-19.

Morel, L. 2004. Mouse models of human autoimmune diseases: essential tools that require the proper controls. *PLoS Biol*. 2:E241.

Morin, P.J. 2005. Claudin proteins in human cancer: promising new targets for diagnosis and therapy. *Cancer Res*. 65:9603-6.

Morita, K., M. Furuse, K. Fujimoto, and S. Tsukita. 1999a. Claudin multigene family encoding four-transmembrane domain protein components of tight junction strands. *Proc Natl Acad Sci U S A*. 96:511-6.

Morita, K., H. Sasaki, K. Fujimoto, M. Furuse, and S. Tsukita. 1999b. Claudin-11/OSP-based tight junctions of myelin sheaths in brain and Sertoli cells in testis. *J Cell Biol*. 145:579-88.

Morrow, C.M., D. Mruk, C.Y. Cheng, and R.A. Hess. 2010. Claudin and occludin expression and function in the seminiferous epithelium. *Philosophical transactions of the Royal Society of London. Series B, Biological sciences*. 365:1679-96.

Mruk, D.D., and C.Y. Cheng. 2004. Sertoli-Sertoli and Sertoli-germ cell interactions and their significance in germ cell movement in the seminiferous epithelium during spermatogenesis. *Endocr Rev*. 25:747-806.

Neaves, W.B. 1973. Permeability of Sertoli cell tight junctions to lanthanum after ligation of ductus deferens and ductuli efferentes. *The Journal of cell biology*. 59:559-72.

Nei, M., P. Xu, and G. Glazko. 2001. Estimation of divergence times from multiprotein sequences for a few mammalian species and several distantly related organisms. *Proc Natl Acad Sci U S A*. 98:2497-502.

O'Donnell, L., K. Pratis, P.G. Stanton, D.M. Robertson, and R.I. McLachlan. 1999. Testosterone-dependent restoration of spermatogenesis in adult rats is impaired by a 5alpha-reductase inhibitor. *Journal of andrology*. 20:109-17.

O'Shaughnessy, P.J., G. Verhoeven, K. De Gendt, A. Monteiro, and M.H. Abel. 2010. Direct action through the sertoli cells is essential for androgen stimulation of spermatogenesis. *Endocrinology*. 151:2343-8.

Oakberg, E.F. 1956. Duration of spermatogenesis in the mouse and timing of stages of the cycle of the seminiferous epithelium. *Am J Anat*. 99:507-16.

Ohta, H., T. Yamaguchi, B.K. Rajapakshage, M. Murakami, N. Sasaki, K. Nakamura, S.J. Hwang, M. Yamasaki, and M. Takiguchi. 2011. Expression and subcellular

localization of apical junction proteins in canine duodenal and colonic mucosa. *American journal of veterinary research*. 72:1046-51.

Park, H.S., G.Y. Kim, I.W. Choi, N.D. Kim, H.J. Hwang, Y.W. Choi, and Y.H. Choi. 2012. Inhibition of Matrix Metalloproteinase Activities and Tightening of Tight Junctions by Diallyl Disulfide in AGS Human Gastric Carcinoma Cells. *J Food Sci*. 76:T105-T111.

Pelletier, R.M., and D.S. Friend. 1983. The Sertoli cell junctional complex: structure and permeability to filipin in the neonatal and adult guinea pig. *Am J Anat*. 168:213-28.

Ribbert, H. 1904. Die Abscheidung intravenös injizierten gelösten Karmins in den Geweben. *Zeitschrift für Allgemeine Physiologie* 4:201-214.

Russell, L. 1977. Movement of spermatocytes from the basal to the adluminal compartment of the rat testis. *Am J Anat*. 148:313-28.

Russell, L.D., A. Bartke, and J.C. Goh. 1989. Postnatal development of the Sertoli cell barrier, tubular lumen, and cytoskeleton of Sertoli and myoid cells in the rat, and their relationship to tubular fluid secretion and flow. *Am J Anat*. 184:179-89.

Schneeberger, E.E., and R.D. Lynch. 2004. The tight junction: a multifunctional complex. *Am J Physiol Cell Physiol*. 286:C1213-1228.

Shum, W.W., N. Da Silva, M. McKee, P.J. Smith, D. Brown, and S. Breton. 2008. Transepithelial projections from basal cells are luminal sensors in pseudostratified epithelia. *Cell*. 135:1108-17.

Stern, L., B. Gold, and N.B. Hecht. 1983. Gene expression during mammalian spermatogenesis. I. Evidence for stage-specific synthesis of polypeptides in vivo. *Biology of reproduction*. 28:483-96.

Sukumar, S.V., and S.L. Kominsky. 2012. Claudins as markers for early detection, diagnosis, prognosis and as targets of therapy for breast and metastatic brain or bone cancer USPTO, editor. The Johns Hopkins University, United States. 2.

Takashima, S., M. Kanatsu-Shinohara, T. Tanaka, M. Takehashi, H. Morimoto, and T. Shinohara. 2011. Rac mediates mouse spermatogonial stem cell homing to germline niches by regulating transmigration through the blood-testis barrier. *Cell Stem Cell*. 9:463-75.

Tsukita, S., and M. Furuse. 2000. Pores in the wall: claudins constitute tight junction strands containing aqueous pores. *J Cell Biol*. 149:13-6.

Tsukita, S., M. Furuse, and M. Itoh. 2001. Multifunctional strands in tight junctions. *Nat Rev Mol Cell Biol*. 2:285-293.

Tsukita, S., Y. Yamazaki, T. Katsuno, and A. Tamura. 2008. Tight junction-based epithelial microenvironment and cell proliferation. *Oncogene*. 27:6930-8.

Verhoeven, G., A. Willems, E. Denolet, J.V. Swinnen, and K. De Gendt. 2010. Androgens and spermatogenesis: lessons from transgenic mouse models. *Philos Trans R Soc Lond B Biol Sci*. 365:1537-56.

Vornberger, W., G. Prins, N.A. Musto, and C.A. Suarez-Quian. 1994. Androgen receptor distribution in rat testis: new implications for androgen regulation of spermatogenesis. *Endocrinology*. 134:2307-16.

Walker, W.H. 2010. Non-classical actions of testosterone and spermatogenesis. *Philosophical transactions of the Royal Society of London. Series B, Biological sciences*. 365:1557-69.

Wang, X., H. Ouyang, Y. Yamamoto, P.A. Kumar, T.S. Wei, R. Dagher, M. Vincent, X. Lu, A.M. Bellizzi, K.Y. Ho, C.P. Crum, W. Xian, and F. McKeon. 2011. Residual embryonic cells as precursors of a Barrett's-like metaplasia. *Cell*. 145:1023-35.

Weber, J.E., and L.D. Russell. 1987. A study of intercellular bridges during spermatogenesis in the rat. *Am J Anat*. 180:1-24.

Willems, A., S.R. Batlouni, A. Esnal, J.V. Swinnen, P.T. Saunders, R.M. Sharpe, L.R. Franca, K. De Gendt, and G. Verhoeven. 2010. Selective ablation of the androgen receptor in mouse sertoli cells affects sertoli cell maturation, barrier formation and cytoskeletal development. *PloS one*. 5:e14168.

Wolburg, H., K. Wolburg-Buchholz, J. Kraus, G. Rascher-Eggstein, S. Liebner, S. Hamm, F. Duffner, E.H. Grote, W. Risau, and B. Engelhardt. 2003. Localization of claudin-3 in tight junctions of the blood-brain barrier is selectively lost during experimental autoimmune encephalomyelitis and human glioblastoma multiforme. *Acta Neuropathol*. 105:586-92.

Wong, C.H., and C.Y. Cheng. 2005. The blood-testis barrier: its biology, regulation, and physiological role in spermatogenesis. *Curr Top Dev Biol*. 71:263-96.

Xavier, R.J., and D.K. Podolsky. 2007. Unravelling the pathogenesis of inflammatory bowel disease. *Nature*. 448:427-34.

Yoshinaga, K., S. Nishikawa, M. Ogawa, S. Hayashi, T. Kunisada, and T. Fujimoto. 1991. Role of c-kit in mouse spermatogenesis: identification of spermatogonia as a specific site of c-kit expression and function. *Development*. 113:689-99.

Zhou, Q., R. Nie, Y. Li, P. Friel, D. Mitchell, R.A. Hess, C. Small, and M.D. Griswold. 2008. Expression of stimulated by retinoic acid gene 8 (Stra8) in spermatogenic cells induced by retinoic acid: an in vivo study in vitamin A-sufficient postnatal murine testes. *Biology of reproduction*. 79:35-42.

Zhou, Q., R. Nie, G.S. Prins, P.T. Saunders, B.S. Katzenellenbogen, and R.A. Hess. 2002. Localization of androgen and estrogen receptors in adult male mouse reproductive tract. *J Androl*. 23:870-81.

VITA

Benjamin Smith was born in Portland, Maine and grew up in both Cape Elizabeth, Maine and Waterford, Maine. At the University of Southern Maine, he earned a Bachelor of Arts degree in Biotechnology with minors in biochemistry and physics. In 2012, he earned a Doctorate of Philosophy at the University of Washington in Genome Sciences.